UMN-TH-1913/00
TPI-MINN-00/35
astro-ph/0007081
June 2000

# On the Determination of the $^4$He Abundance in Extragalactic H II Regions

Keith A. Olive[1,2], and Evan D. Skillman[2]

[1] *Theoretical Physics Institute, University of Minnesota, Minneapolis, MN 55455*
[2] *School of Physics and Astronomy, University of Minnesota, Minneapolis, MN 55455*

**Abstract**

Of the light element abundances capable of testing standard big bang nucleosynthesis, only $^4$He is measured with an accuracy of a few percent. Thus, it is imperative to establish a comprehensive technique for determining $^4$He abundances and reliable estimates of the true systematic uncertainties. Helium abundance determinations in H II regions are made from the observations of several distinct He I emission lines and their strengths relative to H I emission lines. With the general availability of large format, linear CCD detectors, the accuracy of relative emission line ratios has improved to the point where several terms in the error budget which were assumed to be negligible may now be important. Here we investigate the estimation of errors in deriving and reporting nebular helium abundances from optical emission line spectra.

We first investigate the analysis of the H Balmer emission lines. These lines can be used to determine the reddening of the spectrum, but underlying stellar absorption needs to be accounted for. Using a minimization routine, it is possible to solve simultaneously for both reddening and underlying absorption, but, due to the degeneracy of the sensitivities of the individual lines, a minimization routine may underestimate the true errors in the solution. Monte Carlo modeling allows for a better estimate of the errors in underlying absorption and reddening which need to be propagated to all of the data. The magnitude of the $\chi^2$ in such a minimization is important in judging the reliability of the derived solution. We also point out that comparing corrected Balmer line ratios to their theoretical values provides a sensitive test of the propriety of the magnitude of the errors of reported emission line strengths.

The derived $^4$He abundance depends on the H I and He I emissivities, the electron density, the electron temperature, the presence of underlying stellar absorption, and, in some cases, the optical depth in the He I

emission lines. Certain He I emission lines depend sensitively on some of these quantities. Ideally, solutions in which all observable He I lines yield the same answer for the derived He abundance are favored. We examine several methods for such a "self-consistent" analysis to obtain the $^4$He abundance in low metallicity H II regions, and attempt to make a thorough assessment of the uncertainties involved in such determinations. We demonstrate that solving for physical parameters via a minimization routine opens up the possibilities of incorrect solutions if there are any systematic problems with even one observed He I emission line. In many cases, minimizing with just three lines ($\lambda$5876, $\lambda$4471, and $\lambda$6678) is competitive with adding more lines into a minimization (and always provides a useful diagnostic). Underlying He I absorption can be important at the level of reported uncertainties, yet hard to detect. He I $\lambda$4026 is shown to be a sensitive diagnostic of underlying He I absorption, and we recommend adding it in to minimization methods. We show that Monte-Carlo simulations are necessary to reliably determine the uncertainties in the physical parameters as well as the $^4$He abundance determined in minimization routines. We also point out that the magnitude of the $\chi^2$ is important in judging the reliability of the derived solution and should be reported in addition to the derived helium abundance.

## 1. Introduction

The only way to test big bang nucleosynthesis (BBN) and therefore cosmology at an age of order seconds to minutes, is through the observational abundances of the light elements D, $^3$He, $^4$He, and $^7$Li (see. e.g., Olive, Steigman, & Walker 2000). Because there are no measurements of $^3$He at very low metallicity (i.e., significantly below solar) at this time, a higher burden is placed on the remaining three elements. The measurements of D/H in quasar absorption systems are very promising (Burles & Tytler 1998a; 1998b), although not all data agree (Webb et al., 1997; Levshakov, Tytler, & Burles 1998; Tytler *et al.* 1999). Similarly, $^7$Li measurements are continually improving (Ryan, Norris & Beers 1999) and systematic uncertainties are being reduced (Ryan *et al.* 2000), but the accuracy of the primordial abundance determinations for $^7$Li are not probably not much less than a factor of 2. Testing the theory of BBN requires reliable abundances of at least two isotopes. Unlike the other light element abundances, in order to be a useful cosmological constraint, $^4$He needs to be measured with a precision at the few percent level. Thus, the determination of the $^4$He abundance with improved accuracy continues to be of prime importance to cosmology.

To date, the most useful $^4$He abundance determinations are made by observing helium emission lines in HII regions of metal-poor dwarf galaxies. These measurements, which span metallicities ranging down to 1/50th of the solar oxygen abundance, all show $^4$He abundances, $Y$, between 22 and 26% by mass. This is one of the strongest indications that the majority of the $^4$He observed in these systems is in fact primordial and that BBN occurred. At the next level of precision, however, it is necessary to be able to extract a primordial abundance, $Y_p$, from these data (e.g., Pagel et al. 1992, hereafter PSTE). The most common method to determine $Y_p$ is by means of a linear regression with respect to a tracer element (Peimbert & Torres-Peimbert 1974; 1976) such as oxygen or nitrogen (other methods such as a Bayesian analysis gives similar results, Hogan et al. 1997). To first order, we expect that along with the stellar production of heavy elements, there is a component of stellar contamination of primordial He. The uncertainty in the primordial abundance of $^4$He due to this contamination and its exact relationship to the production of heavy elements is reduced by observing the lowest metallicity objects. Currently there is some controversy concerning the best estimate of $Y_p$. Izotov & Thuan (1998b, hereafter IT98) assembled a sample of 45 low metallicity HII regions, observed and analyzed in a uniform manner, and derived a value of $Y_p = 0.244 \pm 0.002$ and $0.245 \pm 0.001$ (with regressions against O/H and N/H respectively). This value is significantly higher than the value of $Y_p = 0.228 \pm 0.005$ derived by PSTE. Analysis based on the combined available data (Olive & Steigman 1995; Olive, Skillman, & Steigman 1997; Fields & Olive 1999) yield an intermediate value of $0.238 \pm 0.002$ with an estimated systematic uncertainty of 0.005. Peimbert, Peimbert, & Ruiz (2000, hereafter PPR) have derived a very accurate helium abundance for the HII region NGC 346 in the Small Magellanic Cloud, and from this they infer a value of $Y_p = 0.2345 \pm 0.0026$. These different results depend, in part, on differences in the analyses of the observations. Thus, it is important to better understand any systematic effects that may result due to different analyses methods. Furthermore, as one can plainly see, the differences in the various determinations of the $^4$He abundance appears to be many sigma. Thus it is clear that present systematic errors have been underestimated, and the main goal

of this paper is to specify methods to better quantify and reduce the systematic uncertainties in $^4$He abundance determinations.

Of course, the degree to which we can make an accurate determination of the primordial He abundance ultimately depends on our ability to extract accurate $^4$He abundances from individual extragalactic HII regions. All of the information comes from the relative strengths of the emission lines of He I and H I, and the emission lines of heavier elements such as oxygen, nitrogen, and sulfur. To determine a $^4$He abundance from the emission line intensities, it is necessary to determine the physical characteristics of the HII region. The electron temperature of the HII region is usually determined from the temperature sensitive ratio of [O III] emission lines (but see PPR). Electron densities can be derived from the ratios of [S II] and [O II] lines, although these may not be favored (see Izotov et al. 1999 and also section 2.4). While the relative H I and He I emissivities have very small dependencies on the electron densities, certain He I emission lines have an enhanced density dependence due to the collisional excitation of electrons out of the metastable 2S state. Additionally, some He I emission lines are subject to enhancement or diminuation through the radiative transfer effects of absorption or florescence.

One also needs to ascertain whether or not neutral helium (or neutral hydrogen) corrections are important (e.g., Shields & Searle 1978; Dinerstein & Shields 1986; Viegas, Gruenwald, & Steigman 2000). Finally, corrections due to possible effects of underlying He I stellar absorption in the spectra must be considered, though in the past, these have usually been neglected. Underlying He I absorption was shown to be an important effect for the NW region of I Zw 18 (Izotov & Thuan 1998a). Skillman, Terlevich, & Terlevich (1998) have demonstrated that the effects of underlying He I absorption may be more important than claimed by IT98 and may explain some of the "anomalous" line ratios observed by them (which led to the rejection of certain objects from the linear regressions used to determine $Y_p$).

In some studies (e.g., Skillman & Kennicutt 1993; Skillman et al. 1994), $^4$He abundances determinations were based on a single emission line at $\lambda$6678. This line was deemed preferable as it is less subject to the effects of collisional enhancement relative to the stronger He I lines at $\lambda$4471 and $\lambda$5876 (cf. Pagel & Simonson 1989). Its proximity to H$\alpha$ also means that the ratio $\lambda$6678/H$\alpha$ is practically unaffected by a reddening correction. However, there is always a danger relying on a single emission line. Fortunately, other He I emission lines are available. The three lines $\lambda$4471, $\lambda$5876, and $\lambda$6678 are all relatively insensitive to density and optical depth effects. This means that, on the one hand, the conversion of these line strengths to a helium abundance can be done with greater certainty. On the other hand, they do not provide a reliable estimate of the either the optical depth or density. The latter is known to make a correction of order 1% to 5% (depending on both the density and the temperature) due to collisional excitations. Nevertheless, one could make a case for using only these lines to determine the helium abundance.

Recently, a "self-consistent" approach to determining the $^4$He abundance was proposed by Izotov, Thuan, & Lipovetsky (1994, 1997, hereafter ITL94, ITL97) by considering the addition of other He lines. First the

addition of $\lambda$7065 was proposed as a density diagnostic, and then, $\lambda$3889 was later added to estimate the radiative transfer effects (since these are very important for $\lambda$7065). This is the method used by IT98 in their most recent estimate of $Y_p$. While this method, in principle, represents an improvement over helium determinations using a single emission line, systematic effects become very important if the helium abundances derived from either $\lambda$3889 or $\lambda$7065 deviate significantly from those derived from the other three lines (see §5).

In this paper, we will attempt to better quantify the true uncertainties in the individual helium determinations in extragalactic HII regions. After a brief discussion of the available observables needed in the determination of $y^+ = \mathrm{He}^+/\mathrm{H}^+$, we present methods for determining the reddening correction, C(H$\beta$), the degree of underlying absorption in H I and He I, and ultimately $y^+$. In addition we will show specifically how various uncertainties in measured quantities affect $y^+$. In section 4, we will describe several alternative methods for deriving the helium abundance based on 3 to 6 emission lines. Here we will investigate the utility of adding a sixth He I line, $\lambda$4026, which may be used to make a quantitative correction for the presence of underlying stellar He I absorption. For various cases based on several emission lines, we will test the minimization procedure (with respect to the recombination values) by calculating Monte Carlo realizations of the input data. This enables us to check the stability of any given solution of the minimization and better estimate the uncertainties in our result. In section 5, we present some examples of synthetic data to demonstrate the power of the method and the dangers of systematic uncertainties in the observed He I line strengths. Our conclusions and prospects for accurate helium determinations will be given in section 6.

The goal of this paper is to explore different analysis methodologies and to promote particular observational and analysis techniques. In the future, we will apply the recommended methods to both new observations and other observations reported in the literature.

## 2. Determination of Physical Parameters

In this section, we will concentrate on the impact of the physical input parameters on He abundance determinations. We will discuss the necessity of obtaining accurate line strengths and the limitations in doing so. We pay special attention to reddening as determined by H I line ratios. The uncertainties in this correction are particularly important as they feed into the uncertainty in all of the subsequent He I line strength determinations. We will also discuss determination of the electron temperature and density.

### 2.1. Measurements of Relative Emission Line Strengths and Errors

With the advent of large format, linear CCD array detectors in the last decade, we are in the best position ever to obtain spectra of emission line objects with the quality and accuracy necessary for helium abundance measurements. While it may seem unnecessary to discuss the measurement of emission line strengths here, this work starts with the assumption that the spectra have been properly calibrated and that errors associated

with that calibration have been taken into account. Targets and standard stars should both be observed close to the parallactic angle in order to minimize atmospheric differential refraction (Filippenko 1982). It is important to observe several standard stars (preferably from the HST spectrophotometric standards of Oke 1990). These standard stars are believed to be reliable to about 1% across the optical spectrum, and thus, this sets a fundamental minimum level of uncertainty in any observed emission line ratio. Observations of both red and blue stars allows a check on the possibility of second-order contamination of the spectrum. Typically, one-dimensional spectra are extracted from long-slit (2-D) observations. Special care needs to be taken setting the extraction aperture width and the aperture should be sufficiently wide that small alignment errors do not give rise to systematic errors (this comes at a cost in signal/noise, but ensures photometric fidelity). Given these potential uncertainties, it is unreasonable to record errors of less than one percent in emission line ratios, regardless of the total number of photons recorded. Of course, multiple independent measurements of the same target provide the best estimates of true observational errors, and existing measurements of this type confirm this minimum error estimate (Skillman et al. 1994).

It should also be noted that it is imperative to integrate under the emission line profile (as opposed to fitting the line with a Gaussian profile). Fitting procedures can introduce systematic differences between high signal/noise and low signal/noise lines. Given the dynamic range of the H I and He I emission lines required to produce an accurate He/H abundance (e.g., the faint He I line $\lambda$6678 is about 1% of H$\alpha$ and He I $\lambda$4026 is less than 2% of H$\beta$), any systematic error between measuring strong and faint lines will have dramatic results. A special challenge is presented by the presence of underlying stellar absorption. The underlying absorption is generally broader than the emission, so quite often, when observed at a resolution of a few Angstroms or better, the H I or He I emission line is sitting in an absorption trough. Measuring all H I and He I emission lines in a consistent manner is important to obtaining a good solution for both the emission strength and the underlying absorption (see next section). Measurements at maximum resolution possible (while still measuring all lines simultaneously) are preferred.

### 2.2. Determination of Reddening and Underlying H I Absorption from Balmer Lines

Because (1) we know the theoretical emissivities of the recombination lines of H I (e.g., Hummer & Storey 1987), (2) the ratios of the H I recombination lines in emission are relatively insensitive to the physical conditions of the gas (i.e., electron temperature and density), and (3) there are a number of H I recombination lines spread through the optical spectrum, it is possible to use the observed line ratios to solve for the line-of-sight reddening of the spectrum (cf., Osterbrock 1989). If one assumes a reddening law ($f(\lambda)$, e.g., Seaton 1979), in principle, it is possible to solve for the extinction as a function of wavelength by measuring a single pair of H I recombination lines. Values of C(H$\beta$), the logarithmic reddening correction at H$\beta$, can be derived from:

$$log\left[\frac{I(\lambda)}{I(H\beta)}\right] = log\left[\frac{F(\lambda)}{F(H\beta)}\right] + C(H\beta)f(\lambda), \quad (1)$$

where $I(\lambda)$ is the intrinsic line intensity and $F(\lambda)$ is the observed line flux corrected for atmospheric extinction. Assuming a reddening law introduces a degree of uncertainty. Studies in our Galaxy have shown that the reddening law exhibits large variations between different lines of sight, but these variations are most important in the ultraviolet (Cardelli, Clayton, & Mathis 1989). Additionally, the total measured extinction can have both Galactic and extragalactic components (and note the added complexity of the shift in wavelength for the reddening law for systems at significant redshift). Note that it is typical that no error is associated with the assumption of a reddening law. Davidson & Kinman (1985) point out that tying the He I emission lines to the nearest pair of bracketing H I lines significantly reduces the impact of assuming a reddening law (i.e., "the interpolation advantage"), but it is unlikely that there is absolutely no error incurred with this assumption.

Underlying stellar absorption will affect the ratios of individual H I line pairs, so, in practice, it is best to measure several H I recombination lines. One can then solve for both the reddening and the stellar absorption underlying the emission lines (e.g., Shields & Searle 1978; Skillman 1985). It is generally assumed that the underlying absorption for the brightest Balmer H I lines is constant in terms of equivalent width. It is not clear how much error is incurred through this assumption, and inspection of stellar spectra shows that it is unlikely to be true for the fainter Balmer emission lines (e.g., H8, H9, and higher). However, one has the observational check of comparing these corrected lines to their theoretical values.

We recommend solving for the reddening and the underlying absorption by minimizing the differences between the observed and theoretical ratios for the three Balmer line ratios H$\alpha$/H$\beta$, H$\gamma$/H$\beta$, and H$\delta$/H$\beta$. Both H7 and H8 are blended with other emission lines, so they cannot be used for this purpose. While the H9 and H10 lines are often not observed with sufficient accuracy to constrain the reddening and absorption, in high quality spectra, the relative strengths of H9 and H10 provide a check on the derived solutions. In Appendix A we describe our method of using a $\chi^2$ minimization routine to determine the best values of C(H$\beta$), the underlying equivalent width of hydrogen absorption ($a_{HI}$), and their associated errors.

Figure 1 is presented for instructional purposes. It shows a comparison of the observed and corrected hydrogen Balmer emission line ratios for three synthetic cases. In constructing this figure, synthetic H I Balmer emission line spectra were calculated assuming an electron temperature (18,000 K), density (100 cm$^{-3}$), and H$\beta$ equivalent width (100 Å). Balmer emission line ratios were derived for three different combinations of reddening and absorption. All emission lines and equivalent widths were given uncertainties of 2%. In the first case, the spectrum was calculated assuming reddening and no underlying absorption. The second case assumes underlying absorption and no reddening. The third case has both. The open circles show the deviations of the original synthesized spectra from the theoretical ratios in terms of the synthesized uncertainties (2% for all lines). Note that reddening and underlying absorption induce corrections in the same direction for all three line ratios, i.e., the H$\alpha$/H$\beta$ line ratio increases for increased reddening and underlying absorption and the bluer Balmer line ratios all decrease for both effects. This covariance results in a degeneracy, thereby decreasing the diagnostic power of the corrections as we will show.

The filled circles in Figure 1 show the results of using the $\chi^2$ minimization routine described in Appendix A. If such a minimization is used, then the $\chi^2$ should be reported. This allows one to make an independent check on the validity of the magnitude of the emission line uncertainties. As one can see, the minimization procedure accurately reproduces the assumed input parameters. In case 1, the minimization found C(H$\beta$) = $0.10 \pm 0.03$ and $a_{HI} = 0.00 \pm 0.57$. Similarly, for the other two cases, we find C(H$\beta$) = $0.00 \pm 0.03$, $a_{HI} = 2.00 \pm 0.59$ and C(H$\beta$)= $0.10 \pm 0.03$, $a_{HI} = 2.00 \pm 0.59$ respectively. In all three cases, since the data are synthetic, the $\chi^2$ values for the solutions are vanishingly small. Appendix B discusses cases from the literature where the $\chi^2$ values are quite large, indicating either a problem with the original spectrum, an underestimate of the emission line uncertainties, or both.

As a test to determine the appropriateness of the uncertainties for the values of C(H$\beta$) and $a_{HI}$ as produced by the $\chi^2$ minimization, we have run Monte Carlo simulations of the hydrogen Balmer ratios. The Monte Carlo procedure is described in Appendix A. Figure 2 shows the results of Monte Carlo simulations of solutions for the reddening and underlying absorption from hydrogen Balmer emission line ratios for three synthetic cases based on the input parameters of case 3 of Figure 1. That is, the original input spectra had reddening with C(H$\beta$) = 0.1 and $a_{HI} = 2$ Å. For these values of C(H$\beta$) and $a_{HI}$, we have run the Monte Carlo for three choices of EW(H$\beta$) = 50, 100, and 200 Å. (EW(H$\beta$) = 100 was used in Figure 1). Let us first concentrate on the results shown in the bottom panel of Figure 2. Each small point is the minimization solution derived from a different realization of the same input spectrum (with 2% errors in both emission line flux and equivalent width). The large open point with error bars shows the mean result with $1\sigma$ errors derived from the $\chi^2$ solution from the original synthetic spectrum. The large filled point with error bars shows the mean result with $1\sigma$ errors derived from the dispersion in the Monte Carlo solutions. Note that the covariance of the two parameters leads to error ellipses. The Monte Carlo simulations find the correct solutions, but the error bars appropriate to these solutions are significantly larger than the errors inferred from the single $\chi^2$ minimization. In this case there is a small offset in the mean solutions (mostly due to the fact that solutions with negative values are not allowed). In the bottom panel, the errors in C(H$\beta$) are 29% larger and the errors in $a_{HI}$ are about 61% larger for the Monte Carlo simulations compared to the single $\chi^2$ minimization.

The middle and top panels of Figure 2 show cases for decreasing emission line equivalent width. Note that, given the input assumptions, the constraints on the underlying absorption are stronger in absolute terms for the lower emission line equivalent width cases. In all three cases, the $\chi^2$ minimization errors are smaller than those produced by the Monte Carlo simulations. For the middle panel, the differences are 41% for C(H$\beta$) and 80% for $a_{HI}$, while for the top panel, the differences are 46% for C(H$\beta$) and 86% for $a_{HI}$.

These test cases have shown that the errors in C(H$\beta$) and the underlying stellar absorption can be underestimated by simply using the output from a $\chi^2$ minimization routine, and that Monte Carlo simulations can be used to give a more realistic estimate of the errors. Based on this experience, we recommend that the best way to determine the true uncertainties in the derived values of C(H$\beta$) and $a_{HI}$ is to run Monte Carlo simulations of the hydrogen Balmer ratios. Simply running a $\chi^2$ minimization will underestimate the uncertainty (due, in

large part, to the covariance of the two parameters being solved for). Since the reddening correction must be applied to the He I lines as well, this uncertainty will propagate into the final estimation of the He abundance. This uncertainty, we find, is too large to be ignored.

If He I lines are observed at a given wavelength $\lambda$, their intensities relative to H$\beta$ after the reddening correction is given by eq. (1). The ratios $I(\lambda)/I(H\beta)$ can then be used self-consistently to determine the He abundance and the physical parameters describing the HII regions, after the effects of collisional excitation, florescence, and underlying absorption as described in the next section. We can quantify the contribution to the overall He abundance uncertainty due to the reddening correction by propagating the error in eq. (1). Ignoring all other uncertainties in $X_R(\lambda) = I(\lambda)/I(H\beta)$, we would write

$$\frac{\sigma_X}{X} = \ln 10 \; f(\lambda) \; \sigma_{C(H\beta)} \tag{2}$$

In the examples discussed above, $\sigma_{C(H\beta)} \sim 0.04$ (from the Monte Carlo), and values of $f$ are 0.237, 0.208, 0.109, -0.225, -0.345, -0.396, for He lines at $\lambda\lambda$3889, 4026, 4471, 5876, 6678, 7065, respectively. For the bluer lines, this correction alone is 1 – 2 % and must be added in quadrature to any other observational errors in $X_R$. For the redder lines, this uncertainty is 3 – 4 %. This represents the *minimum* uncertainty which must be included in the individual He I emission line strengths relative to H$\beta$. Note that these errors alone equal or exceed the 2% errors in the individual line strengths assumed for this exercise. However, the magnitude of the reddening error terms for the red lines can be reduced if these lines are compared directly to H$\alpha$. If the corrected H$\alpha$/H$\beta$ ratio is identical to the theoretical ratio, then it would be allowable to include only the uncertainty in the reddening difference between H$\alpha$ and the red He I emission line. On the other hand, it is frequently the case that the corrected H$\alpha$/H$\beta$ ratio is significantly different from the theoretical ratio.

Finally, we should note that an additional complication is the possibility that, in the highest temperature (lowest metallicity) nebulae, the H$\alpha$ line may be collisionally enhanced (Davidson & Kinman 1985; Skillman & Kennicutt 1993). In their detailed modeling of I Zw 18, Stasinska & Schaerer (1999) have found this to be an important effect (of order 7% enhancement in H$\alpha$). If this is not accounted for, this has the effect of artificially increasing the determined reddening (and thus, artificially decreasing the helium abundances measured from the lines redward of H$\beta$ (e.g., $\lambda\lambda$ 5876, 6678) and increasing the helium abundances measured from lines blueward of H$\beta$ (e.g., $\lambda$4471). More work along the lines Stasinska & Schaerer (1999) with photoionization modeling of high temperature nebulae is needed to determine whether this effect is common in these low metallicity regions.

### 2.3. Electron Temperature Determinations from Collisionally Excited Lines

Since the temperature is governed by the balance between the heating and cooling processes, and since the cooling is governed by different ionic species in different radial zones, one expects different ions to have different mean temperatures (cf. Stasińska 1990; Garnett 1992). While this is best treated with a complete photoionization model, a reasonable compromise is to treat the spectrum as if it arose in two different tem-

perature zones, roughly corresponding to the $O^+$ and $O^{++}$ zones. Since the oxygen ions play a dominant role in the cooling, this is a reasonable thing to do. Deriving temperatures in the high ionization zone generally consists of measuring the highly temperature sensitive ratio of the emission from the "auroral line" of [O III] ($\lambda$4363) relative to the emission from the "nebular lines" of [O III] ($\lambda\lambda$4959,5007). Temperatures for the low ionization zone are usually derived from photoionization modeling (e.g., PSTE); although it is possible to derive temperatures in the low ionization zone from the [O II] I($\lambda$7320 + $\lambda$7330)/I($\lambda$3726 + $\lambda$3729) ratio and a similar ratio for [S II] (e.g., González-Delgado et al. 1994; PPR).

Note that, to date, usually only the temperature from the high ionization zone is used to derive the He abundance, and the He which resides in the low ionization zone is generally not dealt with in a self-consistent manner. To estimate the potential size of this effect, we can look at the data for SBS1159+545 from IT98. In SBS1159+545, 19% of the oxygen is in the $O^+$ state (and thus 81% in the $O^{++}$ state). Assuming all of the gas to be at a temperature of 18,400 K (the [O III] temperature), a $\lambda$5876/H$\beta$ ratio of 0.101 $\pm$ 0.002 yields a helium abundance of 0.0855 (before reduction to account for collisional enhancement and in agreement with IT98). Assuming 81% of the gas to be at the [O III] temperature of 18,400 K and 19% of the gas to be at the [O II] temperature of 15,200 K results in a helium abundance of 0.0848, or a difference of 0.8%. While this is a small difference, it is not negligible when compared to the reported uncertainty in the measurement. Curiously, including the effects of collisional enhancement almost perfectly cancels this effect for the reported density of 110 cm$^{-3}$ ($y^+ = 0.0815$ treated as a single temperature zone and $y^+ = 0.0811$ treated as two temperature zones for this object). Thus, using a lower temperature for the $y^+$ in the $O^+$ zone can increase or decrease the helium abundance depending on the density. The main point here is that the temperatures used for the two zones and the helium abundance should be treated consistently (as emphasized by PPR).

Steigman, Viegas, & Gruenwald (1997) have investigated the effect of internal temperature fluctuations on the derived helium abundances and find this to be important in the high temperature regime. The presence of temperature fluctuations, when analyzed assuming no temperature fluctuations, results in underestimating both the oxygen and helium abundances (here only [S II] densities are used, which are typically higher than the densities derived from He I lines). Assuming a range of relatively large temperature fluctuations (with a maximum of 4000K) results in an overall shift in the derived primordial helium abundance of about 3%. Steigman et al. have argued that, in absence of constraints on the temperature fluctuations, the errors should be increased to account for this uncertainty.

Peimbert, Peimbert, & Ruiz (2000) have shown that the different temperature dependences of the He I emission lines can be used to solve for the density, temperature, and helium abundance simultaneously and self-consistently. They point out that photoionization modeling consistently shows that the electron temperature derived from the [O III] lines is always an upper limit to the average temperature for the He I emission, and thus, assuming the [O III] temperature will always produce an upper limit to the true helium abundance. Here we will not explore the possibility of adding the electron temperature as a free parameter to our minimization routines. This is, in part, because the main motivations are to explore the method promoted by IT98, to

explore the possibility of handling the effects of underlying absorption, and also, because one of our main conclusions, that Monte Carlo modeling is required for a true estimation of the errors will be true regardless of the minimization parameters. Nonetheless, this is a very important result with the implication that most helium abundances reported in the literature to date are really *upper limits*.

### 2.4. Electron Density Determinations from Collisionally Excited Lines

The average density can be derived by measuring the relative intensities of two collisionally excited lines which arise from a split upper level. In the "low density regime" collisional de-excitation is unimportant and all excitations are followed by emission of a photon. The ratio of the fluxes then simply reflects the ratio of the statistical weights of the two levels. In the "high density regime", where the level populations are held at the ratio of their statistical weights, the emission ratio becomes the ratio of the product of the statistical weights and the radiation transition probabilities. In the intermediate regime, near the "critical density" the line ratios are excellent density diagnostics. The best known is that of [S II] $\lambda$6717/$\lambda$6731 which is sensitive in the range from $10^2$ to $10^4$ cm$^{-3}$ and can be observed at moderate spectral resolution. At higher spectral resolution, one can use several other line pairs (e.g., [O II] $\lambda$3726/$\lambda$3729).

In order to convert these line ratios into densities, one needs to know the energy level separations, the statistical weights of the levels, and the radiative and collisional excitation and de-excitation rates. Fortunately, one can use the five-level atom program originally written by De Robertis, Dufour, & Hunt (1987) which has been made generally available within IRAF* by Shaw & Dufour (1995). This program has the additional great advantage that the authors have promised to keep the input atomic data updated.

As emphasized by ITL94, ITL97 and IT98, the [S II] line ratio suffers from two problems as a density diagnostic: (1) it is measuring the density is the low ionization zone, which may apply to less than 10% of the emission in a low metallicity giant HII region, and (2) it is relatively insensitive to density below about 100 cm$^{-3}$. Since the collisional excitation of the He I lines is important at the 1% level down to densities as low as 10 cm$^{-3}$, the [S II] lines are not ideal density indicators (cf. Izotov et al. 1999), and deriving densities directly from the He I lines is, in principle, preferable. This is discussed further in §4. However, calculating the density from the [S II] lines (and other collisionally excited lines) provides an excellent consistency check on the density derived from the He I lines.

---

*IRAF is distributed by the National Optical Astronomy Observatories, which is operated by the Association of Universities for Research in Astronomy, Inc. (AURA) under cooperative agreement with the National Science Foundation.

## 3. Converting Individual He I Lines into He/H Abundances

### 3.1. He I and H I Emissivities

The F(He I)/F(H$\beta$) emission line flux ratios are converted to intrinsic intensity ratios, I(He I)/I(H$\beta$), by correcting for reddening and underlying H I absorption and then incorporating the errors in these corrections (from eq. (2)) into the errors in the line ratios as discussed in section 2.2. These intrinsic line ratios can then be converted to He/H abundance ratios by using the theoretical emissivities calculated from recombination and radiative cascade theory (e.g., Brocklehurst 1971; 1972). Here we use the H I emissivities calculated by Hummer & Storey (1987) and the He I emissivities calculated by Smits (1996). See Appendix C for further details. Normally, uncertainties in the H I and He I emissivities are not included in the error calculations when determining He/H abundance ratios. It is usually assumed that these uncertainties are small in comparison with the other error terms, however, the quoted uncertainties on derived nebular helium abundances are becoming so small that this assumption may no longer be true. We would like to note that there is still a need for a modern assessment of the uncertainties of the calculated He I emissivities. Benjamin, Skillman, & Smits (1999) have estimated that the uncertainty in the input atomic data alone may limit the accuracy to 1.5%.

### 3.2. Collisional Enhancement of He I Emission Lines

At the high electron temperatures found in metal poor nebulae, collisional excitation from the metastable 2S level can become significant in determining the higher level populations in He I. This effect has an exponential dependence on electron temperature and a linear dependence on density. Thus, the theoretical emissivities need to be "corrected" for the radiative contribution of these collisional excitations. In order to better calculate these collisional corrections to the radiative cascade, quantum calculations of increasing accuracy have been carried out to determine more exact collisional rates (Berrington et al. 1985; Berrington & Kingston 1987; Sawey & Berrington 1993). Here we use the collisional rates of Sawey & Berrington (1993) and the resulting collisional corrections calculated by Kingdon & Ferland (1995). In principle, it is better to join the collisional effects directly into the recombination cascade calculation (e.g., as done by Benjamin et al. 1999), but for the present exercise absolute numbers are less important than judging the relative magnitudes of various effects. One of the original motivations for this work was to reproduce the results published in IT98, so we have adopted an identical treatment of the input atomic data.

### 3.3. The Effects of Underlying Stellar Absorption

A potential source of systematic error is the possibility of stellar absorption underlying the helium emission lines. Certainly there are typically many early type stars exciting the observed HII regions, and certainly many of these stars have strong He I absorption lines.

Judging the degree to which underlying stellar absorption is important has been a real problem in the past (e.g., Shields & Searle 1978). Kunth & Sargent (1983) proposed the very simple test of looking for a trend in derived He abundance with EW(He I emission). They found no evidence for this effect in their data (which span approximately the same range in EW(He I emission) as modern day observations). Skillman, Terlevich, & Terlevich (1998) reexamined their data and found evidence for a slight trend in He/H with EW(H$\beta$) implying that underlying absorption may be present at a detectable level. The theoretical modeling results of Olofsson (1995) have also been used as a guide in the past. These models indicated that the EW of $\lambda$4471 in absorption was generally of order 0.1 Å or less. However, Skillman, Terlevich, & Terlevich (1998) pointed out that the model results may not be representative of the typical extragalactic HII region observed for these purposes, and that the underlying absorption values may be much larger than 0.1. They also drew attention to an inconsistency in the relative strengths of He I absorption lines modeled by Olofsson. That is, in observed stars (e.g., Lennon et al. 1993) and in numerical models (e.g., Auer & Mihalas 1972), the strengths of the $\lambda$4471 and $\lambda$4026 lines are about a factor of two stronger than $\lambda$4387 and $\lambda$4922, while in the models of Olofsson, the opposite is true. This potentially implies that the underlying absorption in $\lambda$4471 and $\lambda$4026 could have been underestimated by a factor of 4 in Olofsson's models (EWs for $\lambda$5876 and $\lambda$6678 are not calculated). Revisiting the modeling by Olofsson with a view to the specific case of determining nebular helium abundances remains a valuable exercise for the future.

What are the greater implications for this realization that the effects of underlying absorption could have been underestimated in the past? Izotov & Thuan (1998a) have demonstrated that underlying absorption is important in the NW component of I Zw 18. IT98 recognize the potential importance of underlying stellar absorption. They deal with this effect by (1) averaging over three lines or (2) excluding a line from consideration when "absorption is evidently important".

Here, we feel that a truly self-consistent approach will account for the effects of underlying absorption through detection and correction for such effects. In the next section we present a method for doing this. We pursue two different methods; first we include the possibility of underlying absorption in a $\chi^2$ minimization routine. Second, we experiment with including a sixth line $\lambda$4026, which has enhanced sensitivity to underlying absorption.

In order to do this correctly, one must know, a priori, the relative strengths of the underlying He I absorption lines. We assume that the underlying He I stellar absorption lines are all equal in terms of equivalent width. Recall that we made a similar assumption in the case of underlying H I absorption. Similarly, we cannot estimate how much systematic error we are incurring with this assumption in the analysis of real observations. However, by making the same assumption in both the synthesized spectra and the analysis, we can focus on the uncertainties in the method. The assumption of identical equivalent widths is probably not too bad. Observations of individual Galactic B supergiants (Lennon, Dufton, & Fitzsimmons 1993) show that the EW of the absorption lines of $\lambda$6678, $\lambda$4471, and $\lambda$4026 are all of approximately equivalent strength and share the same dependency on stellar effective temperature. The models by Auer & Mihalas (1972) show relatively good

agreement for EW($\lambda$4026), EW($\lambda$4471), EW($\lambda$5876), and EW($\lambda$6678) for temperatures in excess of 35,000 K and surface gravity values values of log g = 4 and 4.5.

### 3.4. He I Optical Depth Effects

In order to compare observational measurements of helium line intensities with theoretical values, it is necessary to consider radiative transfer effects and to determine what effects these have on the resulting line ratios. The standard references for radiative transfer in He I emission lines are those of Robbins (1968) and Robbins & Bernat (1973). Recent examinations of this issue are given by Almog & Netzer (1989), Proga, Mikolajewska, & Kenyon (1994) and Sasselov & Goldwirth (1995). Given the improvements in the atomic data afforded by the re-examination of A-values (Kono & Hattori 1984), the recombination rates (Smits 1996), and collisional rates (Sawey & Berrington 1993), a re-examination of radiative transfer issues should be very useful. For the purpose of reproducing the IT98 results, here we will adopt the fits given by IT98 to the modeling results of Robbins (1968) (the IT98 equations are reproduced in Appendix C). In Figure 3 we show the data from Robbins (1968) and the IT98 fits. Note that for the regime of low values of $\tau(3889)$ relevant for the current study (values of $\tau(3889) \geq 1.5$ are rarely observed) there is very little data available from Robbins (1968). It is also important to note that these results represent only one set of physical conditions. An important parameter is the velocity gradient of the absorbing gas, which has been assumed to be zero in the models chosen by IT98. This is further motivation for a new study of the He I radiative transfer effects.

### 3.5. Ionization Correction Factors

The degree to which the hydrogen and helium ionization zones in an HII region coincide is generally determined by the hardness of the ionizing radiation field, and may be governed, in part, by geometry (e.g., Osterbrock 1989). Thus, there is always concern that in a specific observation of an HII region that neutral helium is co-existent with ionized hydrogen along the line of sight (see, e.g., discussion in Dinerstein & Shields 1986).

Historically, a correction has been applied to the helium abundances in order to correct for unobserved neutral helium. Vílchez & Pagel (1988), following the ideas of Mathis (1982), used the models of Stasińska (1990) to demonstrate that ratios of ionization fractions of sulfur and oxygen provided an accurate measure of the hardness of the radiation field. Pagel *et al.* (1992) used this technique to determine whether such a correction was necessary. Their proposed methodology consisted of a simple test: if the radiation field was soft enough that a significant correction for neutral helium was implied, this correction was probably too uncertain for the proposed candidate to be useful for a helium abundance measurement.

ITL94 and ITL97 applied neutral helium corrections based on the models of Stasińska (1990), without adopting the methodology of PSTE. Unfortunately, the correction derived in ITL94 is based only on the

neutral helium fraction and does not take into account the neutral hydrogen fraction (see discussion in Skillman, Terlevich, & Terlevich 1998). IT98 revised these estimates assuming ionization correction factors of one.

Viegas, Gruenwald, & Steigman (2000) have produced photoionization models indicating that H II regions ionized by young, hot, metal-poor stars may actually have more extended ionized helium regions when compared to the ionized hydrogen. This results in a "reverse" ionization correction, reducing the derived helium abundance by as much as 1% (cf. Figure 2 in Skillman, Terlevich, & Terlevich 1998). At present, lacking observational evidence of this effect, it is not clear that such a correction should be applied, but the fact that it is of order the size of the errors presently quoted on derived helium abundances implies that it should not be ignored in the error budget.

In this work we will simply assume that the ionization correction factors are very close to one. Skillman et al. (1994) noted the constancy of He/H as a function of position in UGC 4483 despite significant variations in oxygen ionization ratios. However, it is very difficult to constrain this uncertainty to less than 1%.

## 4. Self-Consistent Methods for extracting the $^4$He Abundance

Having discussed many of the potential pitfalls in determining the $^4$He abundance in individual extragalactic HII regions, we can now discuss the methodology for making such a determination. As we noted earlier, a He abundance can be inferred for each He I emission line observed by comparing the ratio of its observed intensity to H$\beta$ with the theoretical ratio and correcting for the effects of collisional excitation, florescence and underlying He I absorption. Thus, as per the discussion of the previous sections, we need to determine three physical parameters, the density, $n$, the optical depth, $\tau$, and the equivalent width for underlying helium absorption, $a_{HeI}$. As argued by ITL94 and ITL97, a self-consistent determination of the parameters, if possible, is preferable. Below we describe a few possible methods for such a determination and stress the need for a careful accounting of the resulting errors, which we deem requires a Monte Carlo simulation of the data.

As we noted above and discuss in detail below, different He I lines are more or less sensitive to the different physical parameters. In principle, it is possible to fix these parameters by minimizing $\chi^2$ using only the three best determined line strengths, $\lambda$4471, $\lambda$5876 and $\lambda$6678. However, because these line strengths are not very sensitive to any of the physical parameters of interest, it may be preferable to consider two or even more additional wavelengths. We describe these various possibilities below. Once the parameters and their associated uncertainties have been fixed, the He abundance may be determined by averaging over all of the He I lines used in the determination of the physical parameters.

We note that we are adopting a different philosophical approach here compare to that in IT98. In the final calculation of $y^+$, IT98 use only the main three lines to obtain the final He abundance. Additionally, they adopt and report a minimum density of 10 cm$^{-3}$ (reduced from the minimum density of 50 cm$^{-3}$ adopted in ITL97) and not lower densities which may be derived from their minimizations. To be truly "self-consistent"

would imply that the helium abundance is derived from all observed lines and the physical parameters are those resulting from the minimization. An inspection of the IT98 data reveals that often the He/H ratios derived from the $\lambda$7065 and $\lambda$3889 lines are significantly different from the He/H ratios derived from the main three lines. Additionally, when their minimization routine is applied, one often finds unrealistically small values of the density. We take these as warning signs that in some cases either the minimization is not finding the best possible solution due to a degeneracy in the $\chi^2$ minimization, or there are problems with the input data. In such cases, it makes sense to either reject the object from derivations of the primordial helium abundance or to attribute a larger uncertainty to account for the lack of self-consistency in the minimization solution.

We begin our discussion of the merits of various minimization routines by examining the dependence of the line strengths (for the six He I lines of interest) on the physical parameters, $n, \tau$, and $a_{HeI}$. Figure 4 shows six He I emission lines and their relative dependences on the different effects discussed in the last sections. We show the relative effects for a baseline model of T = 15,000K, $n$ = 10 cm$^{-3}$, $\tau = 0$, and no underlying stellar He I absorption ($a_{HeI} = 0$). The top panel of Figure 4 shows the effects of an error of 500 K. This is of order or larger than the errors typically quoted for electron temperatures for high quality spectra. It can be seen that reasonable errors in electron temperature (or temperature fluctuations) will have a relatively small effect on the derived He/H abundances (note, however, that Peimbert, Peimbert, & Ruiz 2000 have found that a coupling between temperature and density allows solutions with small differences in temperature to result in significant differences in density resulting in larger than expected changes in the derived helium abundance).

The second panel from the top in Figure 4 shows the effect of increasing the density from 10 to 100 and the subsequent collisional enhancement of the He I lines. Clearly, of the six lines, $\lambda$7065 is most sensitive to this effect. Of the three lines normally used to calculate He/H abundances, $\lambda$5876 is the most sensitive and $\lambda$6678 is the least sensitive. $\lambda$7065 would be an ideal density diagnostic if not for the sensitivity to optical depth shown in the third panel.

The third panel from the top in Figure 4 shows the effect of increasing the optical depth $\tau$(3889) from zero to one. $\lambda$7065 has a strong sensitivity to optical depth effects. $\lambda$3889 is also sensitive to $\tau$(3889), and in the opposite sense, so that in combination these two lines could act to constrain both density and optical depth. Unfortunately, $\lambda$3889 is blended with H8 ($\lambda$3890). Thus, in order to derive an accurate F($\lambda$3889)/F(H$\beta$) ratio, the F($\lambda$3890) must be subtracted off and underlying stellar H I (and He I) absorption must be corrected for. This generally implies a relatively large uncertainty for F($\lambda$3889), and thus, a larger uncertainty in the density and optical depth measures than one would hope for.

Finally, the bottom panel in Figure 4 shows the effects of 0.2 Å of underlying stellar absorption. The difference of a factor of three between the effect on $\lambda$5876 and $\lambda$4471 and $\lambda$6678 means that there is some sensitivity to underlying absorption through the analysis of just those three lines. However, the effect is very strong for the weaker $\lambda$4026 line. Thus, we will explore the possibility of adding $\lambda$4026 as a diagnostic line.

It is very important to note from Figure 4 the strong trade-off between density and underlying He I

absorption. All six He I line strengths are increased by increasing the density, while all six He I line strengths are decreased by increasing the underlying He I absorption. While the relative effects vary from line to line, the main result is a basic trade-off between density and underlying absorption when both are included in a minimization routine. This means that adding underlying absorption as a free parameter in a minimization routine will open up a larger range of parameter space for good solutions. On the other hand, it means that if absorption is not included in minimizations, its effects may be masked by driving the solutions to lower He abundances or densities.

### 4.1. Using 3 Lines

In principle, under the assumption of small values for the optical depth $\tau(3889)$, it is possible to use only the three bright lines $\lambda$4471, $\lambda$5876, and $\lambda$6678 and still solve self-consistently for He/H, density, and $a_{HeI}$. Of course, because these lines have relatively low sensitivities to collisional enhancement, the derived uncertainties in density will be large. However, as we will show, if there is some reason to suspect a problem with any of the additional lines, the three line method can actually lead to a more accurate result, and hence should be used as a diagnostic if nothing else. Using a minimization routine, as opposed to a direct solution, it is not even necessary to assume that $\tau(3889) = 0$ in order to derive a helium abundance from just three lines.

The detailed procedure we use to determine the physical parameters along with the He abundance is given in Appendix C. The procedure is actually independent of the number of lines used, though when using fewer lines (as in the present case of 3 lines) the results are likely to be less robust.

### 4.2. Using 5 Lines

A self-consistent approach to determining the $^4$He abundance was proposed by Izotov, Thuan, & Lipovetsky (1994,1997) by considering the addition of other He lines. First the addition of $\lambda$7065 was proposed as a density diagnostic and then, $\lambda$3889 was later added to estimate the radiative transfer effects (since these are important for $\lambda$7065). By minimizing the difference between the ratios of $\lambda$3889/$\lambda$4471, $\lambda$5876/$\lambda$4471, $\lambda$6678/$\lambda$4471, and $\lambda$7065/$\lambda$4471 and their recombination values, the density, optical depth, and helium abundance can be determined. The latter is determined by a weighted mean of the helium abundance based on $\lambda$4471, $\lambda$5876, $\lambda$6678 once the values of $n$ and $\tau(3889)$ are fixed. This is the method used by IT98 in their most recent estimate of $Y_p$. Underlying He I absorption is assumed to be negligible in their method.

While this method, in principle, represents an improvement over helium determinations using a single emission line, systematic effects become very important if the helium abundances derived from either $\lambda$3889 or $\lambda$7065 deviate significantly from those derived from the other three lines. In addition, working with the ratios of all of the He I lines to a single He I line puts undue weight on that single line (in this case $\lambda$4471). This is especially vulnerable to systematic errors in the presence of undetected underlying stellar absorption.

Here, we also consider using these five lines for determining the He abundance along with the physical parameters. However, as described in the appendix B, our minimization procedure is based on the weighted average of the He abundance as determined from the five lines *independently*. We allow for the presence of underlying He I absorption through the assumption that it will be identical (in terms of equivalent width) for all of the He I lines. In addition, once the physical parameters have been determined by the minimization, all five values of $y^+(\lambda)$ are used in a weighted mean to determine the final $Y^+$.

### 4.3. Using 6 Lines

Adding $\lambda$4026 as a diagnostic line increases the leverage on detecting underlying stellar absorption. This is because the $\lambda$4026 line is a relatively weak line. However, this also requires that the input spectrum is a very high quality one. $\lambda$4026 is also provides exceptional leverage to underlying stellar absorption because it is a singlet line and therefore has very low sensitivity to collisional enhancement (i.e., $n$) and optical depth (i.e., $\tau(3889)$) effects.

Our procedure for this case is identical to the one above with the addition of the sixth line. By adding $\lambda$4026 as a diagnostic line, we increase our dependence on the assumption of equal equivalent width of underlying absorption for all of the He I lines. Our philosophy is that it is most important to discover underlying absorption when it is present. If underlying absorption is important in an individual spectrum, conservatively, it may be better to reject the object from consideration from studies constraining the primordial helium abundance. If a solution implies significant underlying absorption, and all of the helium lines give the same abundance within errors, it may be taken as an endorsement of the assumption of equal EW of underlying He I absorption.

## 5. Test Cases and Examples

In this section we present the results from a number of test cases varying the input physical parameters, the number of He I emission lines used in the minimizations, and assumptions about certain physical parameters. Our philosophy here has been to test for relatively small variations, since the final goal is helium abundances for individual nebulae with accuracies approaching 1%. That is, we are confident that if assumptions are grossly in error that the derived abundances are wrong, but, more importantly, if there is a very subtle effect (e.g., a very small amount of underlying absorption or a small amount of optical depth), we need to understand how that will affect our derived helium abundances.

### 5.1. Cases with no Systematic Errors

We present here the results of running a few series of test cases. In all cases, input spectra were synthesized with the prescriptions and assumptions described above or in the appendices. We chose a baseline model of

T = 18,000 ± 200 K, EW(H$\beta$ = 100), and He/H = 0.080. We then varied the density, $a_{HeI}$, and $\tau(3889)$ to produce different cases. Errors of 2% were assumed for all of the input emission lines and equivalent widths, and then each of these models were run through Monte Carlo realizations. We then analyze the resulting distributions of the results from a $\chi^2$ minimization solution for He/H, density, $a_{HeI}$, and $\tau(3889)$.

Figure 5 presents the results of modeling of 6 synthetic He I line observations for a single case. The four panels show the results of a density = 10 cm$^{-3}$, $a_{HeI} = 0$, and $\tau(3889) = 0$ model. The solid lines show the input values (e.g., He/H = 0.080) for the original calculated spectrum. The solid circles (with error bars) show the results of the $\chi^2$ minimization solution (with calculated errors) for the original synthetic input spectrum. The small points show the results of Monte Carlo realizations of the original input spectrum. The solid squares (with error bars) show the means and dispersions of the output values for the $\chi^2$ minimization solutions of the Monte Carlo realizations.

Figure 5 demonstrates several important points. First, our $\chi^2$ minimization solution finds the correct input parameters with errors in He/H of about 1% (less than the 2% errors assumed on the input data, showing the power of using multiple lines). In this low density case, the Monte Carlo results are in relatively good agreement with the input data, with similar sized error bars. There is a small offset to lower densities and a similar small offset to non-zero values of underlying absorption. We found this effect throughout our modeling, that when an input parameter such as underlying He I absorption or $\tau(3889)$ is set to zero, the minimization models of the Monte Carlo realizations (cases with errors) always found slightly non-zero values (although consistent with zero) in minimizing the $\chi^2$. Note that in the lower right panel of Figure 5 that the values of the $\chi^2$ do not correlate with the values of $y^+$. The solutions at higher values of absorption and $y^+$ are equally valid as those at lower absorption and $y^+$.

Figure 6 presents the results of modeling of 6 synthetic He I line observations for a case identical to that of Figure 5 with the exception of a higher density of 100 cm$^{-3}$. For the $n = 100$ cm$^{-3}$ case, there is a systematic trend for the Monte Carlo realizations to tend toward higher values of He/H. This is because, again, the inclusion of errors has allowed minimizations which find lower values of the density and non-zero values of underlying absorption and optical depth. However, in this case, there is more "distance" from the lower bound of $n = 0$, and thus more parameter space to allow the effects of the parameter degeneracy to be noticed. Note that the size of the error bars in He/H have expanded by roughly 50% as a result. We can conclude from this that simply adding additional lines or physical parameters in the minimization does not necessarily lead to the correct results. In order to use the minimization routines effectively, one must understand the role of the interdependencies of the individual lines on the different physical parameters. Here we have shown that trade-offs in underlying absorption and optical depth allow for good solutions at densities which are too low and resulting in helium abundance determinations which are too high. *This is one of the central results of this study.* Again, note that there is no trend in the values of $\chi^2$ with $y^+$.

Table 1 summarizes the results of a number of different test cases like those shown in Figures 5 and 6.

Table 1 is grouped into six different cases of input with five different minimization routines. The first two cases correspond those shown in Figures 5 and 6. The other four cases consider non-zero values of underlying absorption, $\tau(3889)$, or both. The first two columns show the results of minimizing on 3 lines (both assuming $\tau(3889)$ is zero and solving for $\tau(3889)$). The next two columns show the results of minimizing on 5 lines (both assuming zero underlying absorption and solving for the underlying absorption). The last column shows the results of the six line method which was used to produce Figures 5 and 6.

The numbers in the table correspond to the average of the Monte Carlo results and their dispersion. The row labeled He/H gives the results from averaging the He/H abundances from all of the lines (3, 5 or 6), while the "He/H (3)" row gives the He/H values derived from averaging only the three main He I lines (after solving for the physical parameters). Note that the straight minimizations of the input data always returned the input data (except in the cases where an assumption is inconsistent with the input data). Deviations of the Monte Carlo solutions from the input values result because of: (1) inconsistencies between the input data and input assumptions, (2) asymmetries in the Monte Carlo distributions (e.g., in Figure 5, because the absorption is not allowed to go negative, the distribution is truncated on one side, and thus there is a bias to higher values of $y^+$), (3) degeneracies between different parameters which result in lower $\chi^2$ values for values of the physical parameters quite far from their input values.

For the first two cases, (no underlying absorption and no optical depth), as expected, the 3 line method constraints on the density are not strong. However the derived helium abundances are consistent, within the errors, with the input values. For the 5 line method, since the first two cases (1 and 2) have no underlying absorption, the method with the correct assumption finds a solution much closer to the correct result (although all solutions are consistent with the correct result, within errors). Again, it is the degeneracy between density and underlying absorption which is responsible for the derived low density and high He abundance. Note, interestingly, that the three line method did not do any worse (in fact it did slightly better) than the 5 line methods, unless we assume a priori the correct answer for underlying absorption ($a_{HeI} = 0$). Similarly, assuming $\tau = 0$ also improves the result in this case for obvious reasons. The six line method, within the errors, gave results consistent with but not equal to the input parameters. Indeed, there is a systematic trend to lower density and some underlying absorption even when there is none. The net result is a higher estimate of the He abundance. This systematic trend can be traced to the degeneracy in the trends imposed by the different input parameters. However, the 6 line method does significantly better than the 5 line method at constraining the underlying absorption (as the $\lambda$4206 line anchors the values of $a_{HeI}$).

We learn more about the various methods when we consider the remaining cases in Table 1. When $\tau(3889) \neq 0$ (and $a_{HeI} = 0$), the five and six line methods give very accurate results although, once again, $\lambda$4206 is needed to pin down the value of $a_{HeI}$ and break the degeneracy. When the input value of $a_{HeI} \neq 0$, then only the 5 line method which assumes $a_{HeI} = 0$ does badly. The 5 and 6 line methods which solve for $a_{HeI}$ do quite well. Figure 7 shows the results of the Monte Carlo when both $\tau$ and $a_{HeI} \neq 0$, and $n = 100$ cm$^{-3}$, i.e., case 6 of Table 1. Thus it is encouraging that in perhaps more realistic cases where the input parameters

are non-zero, we are able to derive results very close to their correct values.

Indeed, Figure 7 shows many of effects we have been describing in the previous cases. The average of Monte Carlo realizations is remarkably close to the straight minimization for all of the derived parameters ($n, a_{HeI}, \tau$ and $y^+$). However, there is an enormous dispersion in these results due to the degeneracy in the solutions with respect to the physical input parameters. This results in error estimates for parameters which are significantly larger than in the straight minimization. For example, the uncertainties in both the density and optical depth are almost a factor of 3 times larger in the Monte Carlo. When propagated into the uncertainty in the derived value for the He abundance, we find that the uncertainty in the Monte Carlo result (which we argue is a better, not merely more conservative, value) is a factor of 2.5 times the uncertainty obtained from a straight minimization using 6 line He lines. This amounts to an approximately 4% uncertainty in the He abundance, despite the fact that we assumed (in the synthetic data) 2% uncertainties in the input line strengths. This is an unavoidable consequence of the method - the Monte Carlo routine explores the degeneracies of the solutions and reveals the larger errors that should be associated with the solutions.

From the above, we conclude (1) that adding absorption to the minimization routines can lead to much larger regions of valid solution space; (2) the trivial result that assuming no underlying absorption will lead to incorrect solutions in the presence of underlying absorption, (3) that adding an accurate $\lambda$4026 observation to a minimization solution will provide strong diagnostic power for underlying stellar absorption, and (4) that Monte Carlo models are required to determine the true uncertainties in the minimization results.

### 5.2. Cases with Systematic Errors in I($\lambda$3889)

In §4, it was shown that $\lambda$3889 is strongly sensitive to optical depths effects and is required if $\lambda$7065 is to be a good tracer of density. It was also pointed out that, unfortunately, $\lambda$3889 is blended with H8 ($\lambda$3890). Thus, in order to derive an accurate F($\lambda$3889)/F(H$\beta$) ratio, the F($\lambda$3890) must be subtracted off and underlying stellar H I (and He I) absorption must be corrected for.

In the methodology of IT98, the contribution to He I $\lambda$3889 from H I emission is subtracted off by assuming the theoretical value for the H I emission (typically, the He I emission accounts for almost 50% of the blended line). The total emission has to be corrected for underlying stellar absorption, which is assumed to be a constant equivalent width for all of the H I lines. This assumption is a potentially dangerous one. Spectral studies of individual stars show that while this may be a good assumption to first order, the equivalent widths of the higher order Balmer lines are not strictly identical (see, for example, the spectral atlas of Galactic B supergiants of Lennon, Dufton, & Fitzsimmons 1992). Secondly, this correction is usually large (corrected He I $\lambda$3889 emission line equivalent widths generally lie in the range of 4 to 10Å compared to the underlying absorption which is in the range of 0.5 to 3Å). A good test of the uncertainty in this correction would be a comparison of the corrected higher order (H9 and H10) H I emission line strengths compared to their theoretical values. In Appendix B,

we show a few cases in the literature, where these comparisons reveal evidence of a problem.

Here we investigate the possible effects of a systematically low strength of $\lambda$3889 motivated by the possibility of oversubtracting the underlying H I absorption. We have run identical cases and analyses as in Table 1, but altered the input synthetic spectra by decreasing the relative flux and equivalent width of $\lambda$3889 by 10%. These results are presented in Table 2. The first two columns are identical (since they are based on only three unaffected lines) and are repeated for comparison. Note that this exercise was motivated, in part, by the systematically low values of He/H derived from $\lambda$3889 when compared with the main three He I lines in a subsample of the highest quality data from IT98.

The 10% drop in $\lambda$3889 has dramatic effects. From §4, and especially Figure 4, it can be seen, that an underestimate of I($\lambda$3889) will lead to both artificially high values of $\tau$(3889) and artificially low values of the density. This is born out in inspection of Table 2. Beginning with the cases in which the input values of $\tau$ and $a_{HeI}$ are 0, we see that the density is grossly underestimated in both input cases with $n$ = 10 and 100 cm$^{-3}$. In the low density case, the He/H solutions based on all available lines are low, while the He/H(3) solutions are close to correct. This main effect is due to including the low value of He/H from $\lambda$3889. However, in the high density case, it is the values of He/H(3) which are in error on the high side. This is due to the underestimate of the density (and thus the corrections for collisional enhancement are too small). Note that the solutions for $\tau$(3889) have been driven to large values. For both the higher density cases, the density has been underestimated, the $\tau$(3889) overestimated, and the He/H(3) overestimated.

In Figure 8, we show the results of the 6 line method Monte Carlo for case 2 of Table 2. Here the low density, high $\tau$(3889), and bias towards higher values of He/H are clear (even higher values would be shown if He/H(3) were plotted). Note that the lower right panel shows that the $\chi^2$ values are all systematically high for this case. It would appear that the $\chi^2$ is a sensitive test to check whether the I($\lambda$3889) values are systematically biased.

The low density cases show generally low values of He/H and satisfactory values of He/H(3) (although the solutions for $\tau$(3889) are all systematically high). The main result of a systematically low values of I($\lambda$3889) occurs when the nebula has a high enough density that the collisional enhancement is important. Then the underestimate of density results in systematically higher He/H.

### 5.3. Cases with Systematic Errors in I($\lambda$7065)

One of the possible problems of using $\lambda$7065 is that in a spectrum where the entire wavelength range from $\lambda$3727 to $\lambda$7065 is observed in first order, there is the potential for contamination of the red part of the spectrum from blue light in the second order. In principle, if a blue cutoff filter is used (e.g., a CG385 order separation filter) then there should be little contamination blueward of 2 $\times$ 3850 Å or 7700 Å. However, order separation filters are not perfect cut-on filters at 3850 Å, but rather start to filter out light above 4000 Å, reach

50% transparency at about 3850 Å and then drop to zero transparency somewhere between 3500 and 3600 Å. Thus, there is potential for some second order contamination for all wavelengths above 7000 Å. If the observed target has a significant redshift, then the He I $\lambda$7065 is even more susceptible to this problem. The problem is worse for bluer order separation filters (e.g., CG375).

This effect can be quite subtle and there are two separate problems to consider. The first is contamination of the standard star spectrum. If a blue standard star (e.g., a white dwarf) is used for flux calibration, then the far red part of the spectrum detects additional second order blue photons, which, when used to calibrate the spectrograph, results in an overestimate of the red sensitivity of the spectrograph. The second problem occurs in the target spectrum. Here the far red continuum will be contaminated by extra second order blue photons. It is possible that if the blue spectral shape of the standard star is similar to the spectral shape of the target, then these two effects will compensate, giving a rather normal looking red continuum. However, the overestimate of the red sensitivity will result in underestimated emission line fluxes and equivalent widths. Since $\lambda$7065 lies right at the border of where this effect can become important, it is very important to check for this possibility. This is most easily done by obtaining spectra of both red and blue standard stars and deriving instrument sensitivity curves independently for the two stars. The wavelength at which the two sensitivity curves begin to deviate indicates the onset of second order contamination.

Here we investigate the possible effects of a systematically low strength of $\lambda$7065. We have run identical cases and analyses as in Table 1, but altered the input synthetic spectra by decreasing the relative flux and equivalent width of $\lambda$7065 by 5%. These results are presented in Table 3. Note that this exercise was motivated, in part, by the systematically low values of He/H derived from $\lambda$7065 when compared with the main three He I lines in a subsample of the highest quality data of IT98.

The 5% drop in $\lambda$7065 has dramatic effects. Beginning with the cases in which the input values of $\tau$ and $a_{HeI}$ are 0, we see that the density is grossly underestimated in both input cases with $n = 10$ and 100 cm$^{-3}$. In the low density cases, this does not have a very strong effect on the derived helium abundances (because the density dependent collisional enhancement term is already quite small).

In the high density case with no underlying absorption or optical depth effects, the five and six line methods give a He abundances which are significantly higher than the correct value of 0.08. In this case, the three line method which is not distracted by the errant $\lambda$7065 line does the best at finding the solution. We see the effect of the $\lambda$7065 line driving down the density and compensating by allowing for non-zero absorption, which is controlled in the 6 line method due to $\lambda$4026.

In Figure 9, we show the results of the six-line method Monte Carlo for case 2 of Table 3. Case 2 shows the most discrepant results in Table 3, and the six-line method is only better than the five-line method with absorption allowed (but not constrained by $\lambda$4026. Here it can be seen clearly that the solutions all favor lower density, and thus higher He/H. The trade-off between low density and high values of underlying absorption is clearly shown. Interestingly, the values for $\chi^2$ are relatively low and quite satisfactory. Clearly the $\chi^2$ is not a

good diagnostic of an underestimated I($\lambda$7065), as the degeneracies allow mathematically acceptable solutions.

Case 6 provides an interesting comparison case to consider when $\lambda$7065 is low. Notice here, that the 5 and 6 line methods again over-estimate the He abundance. While both solutions find the approximate underlying absorption (the 6 line method is better) they underestimate the density and the optical depth. Here the 3 line method, even with its lack of sensitivity, still solves for the correct density (to within 8% when $\tau$ is not assumed to be zero) and underlying absorption. The He abundance is again very accurately determined by this method.

In Figure 10, we show the results of the six-line method Monte Carlo for case 6 of Table 3. In this case of a small amount of optical depth and a small amount of underlying absorption, the solutions do a pretty good job of finding the correct range of density, optical depth, and underlying absorption. The underestimated $\lambda$7065 has resulted in a bias toward lower density, which has resulted in a bias toward larger He/H, but the effect is not very large. The main effect is the size of the error bars. Here it is clear that Monte Carlo errors in He/H are about 3 times larger than the errors from a straight minimization. Note again that the $\chi^2$ values are generally small.

The main result of tests with a systematically low $\lambda$7065 is that for nebulae with densities which correspond to significant collisional enhancement corrections, the He/H will be overestimated. The $\chi^2$ is not necessarily a good test of whether $\lambda$7065 has been systematically underestimated.

## 6. Discussion

We have pointed out a number of points in the analysis of optical spectra of nebulae that can lead to biased or inaccurate abundance results if not accounted for properly. We hope to draw attention to the treatment of the H I Balmer lines as a critically important step in an accurate abundance analysis.

Our inspection of self consistent minimization methods for determining helium abundances has revealed several things. In the perfect world when all of the uncertainties in the input data are under control, the 6 line method is best at solving for the physical input parameters and ultimately the He abundance. However, minimization routines should used with caution with a eye toward systematically biased observations. The key diagnostics are the values of the $\chi^2$ in a straight minimization, and the results of the 3 line method. When the data are good the $\chi^2$ per degree of freedom should be small, and the results of the 3, 5, and 6 line methods should be consistent. The latter methods should be more accurate and carry smaller error bars on the derived quantities. If either of these conditions are not met, then it is probably not advisable to use those data in a determination of the primordial He abundance. In any case, a Monte Carlo realization of the observations should be conducted to assess the true uncertainties in the resultant abundances.

While it may seem that, in some cases, the straight minimization gives a solution closer to the original input parameters than does the average Monte Carlo result, one must bear in mind that we have been using synthetic data with known values. By running the Monte Carlo on synthetic data we are modeling possible

sets of observations consistent with the true physical description of the HII region. That is, each Monte Carlo minimization represents the result of a single possible observation. Running a Monte Carlo realization of real data allows an exploration of all of the possible suitable solutions allowed by the degeneracies in the sensitivities of the various He I lines to the different physical parameters.

Clearly the abundances used in estimating $Y_p$ are not observed but rather derived quantities. As we have seen, the derivation of the He abundance relies on several, a priori, unknown but physical input parameters. In this paper, we hope to have clarified the determination process, and quantified the uncertainties in the result. Thus, it may be premature to be arguing over the 3rd decimal place in $Y_p$ until a systematic treatment and Monte Carlo analysis of the data has been performed. Our purpose here is not to propose a minimum error for all nebular helium abundances nor to try to give a quantitative estimate of how a given analysis may result in a systematic bias in the derivation of $Y_p$. Rather, we wish to promote a methodology for the analysis of all nebular HII region spectra in the pursuit of accurate He abundances. We emphasize the importance of reporting more information (the equivalent widths of all of the H I and He I emission lines, the $\chi^2$ results for minimizations) and the use of Monte Carlo techniques for characterizing error terms. In the future, we will apply the recommended methods to both new observations and other observations reported in the literature.

**Acknowledgments**

We would like to thank R. Kennicutt and B. Pagel for insightful comments on the manuscript. We also are pleased to thank R. Benjamin, D. Kunth, M. Peimbert, G. Shields, J. Shields, G. Steigman, E. Terlevich, and R. Terlevich for informative and valuable discussions. The work of KAO is supported in part by DOE grant DE-FG02-94ER-40823. EDS is grateful for partial support from a NASA LTSARP grant No. NAGW-3189.

Table 1. Results From Synthetic Spectra

| Variables | Input | 3 Lines $\tau(\lambda3889) = 0$ | 3 Lines | 5 Lines abs(He i) = 0 | 5 Lines | 6 Lines |
|---|---|---|---|---|---|---|
| | | | Case 1 (B) | | | |
| density | 10 | 34.5±57.0 | 33.9 ± 56.8 | 7.1 ± 12.4 | 5.8 ± 10.9 | 5.0 ± 9.8 |
| $\tau$(3889) | 0.0 | (0.0) | 0.018±0.039 | 0.003 ± 0.007 | 0.003 ± 0.007 | 0.003 ± 0.006 |
| abs(He i) | 0.0 | 0.035±0.059 | 0.037 ± 0.061 | (0.0) | 0.047 ± 0.068 | 0.014 ± 0.021 |
| He/H | 0.080 | 0.0801±0.0018 | 0.0802±0.0018 | 0.0801±0.0009 | 0.0808±0.0013 | 0.0804±0.0009 |
| He/H (3) | 0.080 | 0.0801±0.0018 | 0.0802±0.0018 | 0.0802±0.0011 | 0.0809±0.0014 | 0.0804±0.0011 |
| | | | Case 2 (A) | | | |
| density | 100 | 91.9±92.7 | 90.9 ± 92.5 | 69.4 ± 43.7 | 59.7 ± 44.7 | 58.4 ± 42.8 |
| $\tau$(3889) | 0.0 | (0.0) | 0.028±0.047 | 0.022 ± 0.035 | 0.030 ± 0.041 | 0.029 ± 0.039 |
| abs(He i) | 0.0 | 0.049±0.072 | 0.050 ± 0.074 | (0.0) | 0.059 ± 0.076 | 0.021 ± 0.026 |
| He/H | 0.080 | 0.0811±0.025 | 0.0812±0.0026 | 0.0808±0.0014 | 0.0819±0.0019 | 0.0815±0.0015 |
| He/H (3) | 0.080 | 0.0811±0.025 | 0.0812±0.0026 | 0.0808±0.0015 | 0.0819±0.0020 | 0.0813±0.0017 |
| | | | Case 3 (I) | | | |
| density | 10 | 35.2±57.7 | 34.7 ± 57.5 | 33.7 ± 43.8 | 26.7 ± 40.5 | 22.0 ± 34.2 |
| $\tau$(3889) | 0.1 | (0.0) | 0.020±0.044 | 0.080 ± 0.058 | 0.090 ± 0.058 | 0.091 ± 0.055 |
| abs(He i) | 0.0 | 0.036±0.060 | 0.038 ± 0.062 | (0.0) | 0.038 ± 0.061 | 0.012 ± 0.020 |
| He/H | 0.080 | 0.0802±0.0018 | 0.0802±0.0019 | 0.0795±0.0014 | 0.0802±0.0016 | 0.0801±0.0012 |
| He/H (3) | 0.080 | 0.0802±0.0018 | 0.0802±0.0019 | 0.0796±0.0015 | 0.0803±0.0018 | 0.0800±0.0015 |
| | | | Case 4 (J) | | | |
| density | 10 | 46.1±68.0 | 44.7 ± 67.4 | 9.0 ± 13.5 | 6.5 ± 11.5 | 7.1 ± 11.6 |
| $\tau$(3889) | 0.0 | (0.0) | 0.030±0.052 | 0.002 ± 0.005 | 0.003 ± 0.006 | 0.003 ± 0.006 |
| abs(He i) | 0.1 | 0.094±0.093 | 0.097 ± 0.094 | (0.0) | 0.114 ± 0.097 | 0.101 ± 0.035 |
| He/H | 0.080 | 0.0793±0.0024 | 0.0793±0.0019 | 0.0785±0.0009 | 0.0803±0.0017 | 0.0801±0.0012 |
| He/H (3) | 0.080 | 0.0793±0.0024 | 0.0793±0.0019 | 0.0785±0.0011 | 0.0804±0.0018 | 0.0802±0.0013 |
| | | | Case 5 (H) | | | |
| density | 10 | 47.1±68.7 | 45.6 ± 68.1 | 52.0 ± 50.5 | 32.6 ± 43.9 | 35.0 ± 43.6 |
| $\tau$(3889) | 0.1 | (0.0) | 0.031±0.058 | 0.059 ± 0.057 | 0.082 ± 0.059 | 0.079 ± 0.058 |
| abs(He i) | 0.1 | 0.095±0.093 | 0.097 ± 0.095 | (0.0) | 0.098 ± 0.092 | 0.095 ± 0.037 |
| He/H | 0.080 | 0.0793±0.0024 | 0.0793±0.0024 | 0.0775±0.0015 | 0.0795±0.0020 | 0.0794±0.0017 |
| He/H (3) | 0.080 | 0.0793±0.0024 | 0.0793±0.0024 | 0.0776±0.0016 | 0.0796±0.0022 | 0.0795±0.0019 |
| | | | Case 6 (G) | | | |
| density | 100 | 111±103 | 108±104 | 135±75.5 | 101±75.2 | 105±76.1 |
| $\tau$(3889) | 0.1 | (0.0) | 0.041±0.052 | 0.089 ± 0.096 | 0.140 ± 0.117 | 0.131 ± 0.115 |
| abs(He i) | 0.1 | 0.111±0.104 | 0.115 ± 0.107 | (0.0) | 0.116 ± 0.100 | 0.104 ± 0.041 |
| He/H | 0.080 | 0.0802±0.0031 | 0.0803±0.0032 | 0.0779±0.0019 | 0.0804±0.0028 | 0.0802±0.0025 |
| He/H (3) | 0.080 | 0.0802±0.0031 | 0.0803±0.0032 | 0.0779±0.0020 | 0.0804±0.0029 | 0.0801±0.0026 |

Table 2. Results From Synthetic Spectra with He I $\lambda$3889 10% Low

| Variables | Input | 3 Lines $\tau(\lambda3889) = 0$ | 3 Lines | 5 Lines abs(He i) = 0 | 5 Lines | 6 Lines |
|---|---|---|---|---|---|---|
| | | | Case 1 (B) | | | |
| density | 10 | 34.5±57.0 | 33.9 ± 56.8 | 1.3 ± 2.8 | 1.2 ± 2.2 | 0.1 ± 0.0 |
| $\tau$(3889) | 0.0 | (0.0) | 0.018±0.039 | 0.024 ± 0.022 | 0.025 ± 0.022 | 0.020 ± 0.020 |
| abs(He i) | 0.0 | 0.035±0.059 | 0.037 ± 0.061 | (0.0) | 0.032 ± 0.055 | 0.002 ± 0.006 |
| He/H | 0.080 | 0.0801±0.0018 | 0.0802±0.0018 | 0.0779±0.0008 | 0.0783±0.0011 | 0.0784±0.0007 |
| He/H (3) | 0.080 | 0.0801±0.0018 | 0.0802±0.0018 | 0.0803±0.0010 | 0.0808±0.0012 | 0.0803±0.0010 |
| | | | Case 2 (A) | | | |
| density | 100 | 91.9±92.7 | 90.9 ± 92.5 | 2.6 ± 10.0 | 1.1 ± 4.1 | 1.1 ± 5.8 |
| $\tau$(3889) | 0.0 | (0.0) | 0.028±0.047 | 0.158 ± 0.055 | 0.163 ± 0.053 | 0.156 ± 0.052 |
| abs(He i) | 0.0 | 0.049±0.072 | 0.050 ± 0.074 | (0.0) | 0.053 ± 0.075 | 0.007 ± 0.014 |
| He/H | 0.080 | 0.0811±0.025 | 0.0812±0.0026 | 0.0800±0.0008 | 0.0809±0.0013 | 0.0804±0.0008 |
| He/H (3) | 0.080 | 0.0811±0.025 | 0.0812±0.0026 | 0.0822±0.0010 | 0.0831±0.0015 | 0.0823±0.0011 |
| | | | Case 3 (I) | | | |
| density | 10 | 35.2±57.7 | 34.7 ± 57.5 | 1.2 ± 3.1 | 0.7 ± 1.5 | 1.4 ± 3.9 |
| $\tau$(3889) | 0.1 | (0.0) | 0.020±0.044 | 0.221 ± 0.061 | 0.225 ± 0.063 | 0.208 ± 0.060 |
| abs(He i) | 0.0 | 0.036±0.060 | 0.038 ± 0.062 | (0.0) | 0.032 ± 0.055 | 0.003 ± 0.007 |
| He/H | 0.080 | 0.0802±0.0018 | 0.0802±0.0019 | 0.0779±0.0007 | 0.0784±0.0011 | 0.0783±0.0007 |
| He/H (3) | 0.080 | 0.0802±0.0018 | 0.0802±0.0019 | 0.0803±0.0010 | 0.0808±0.0012 | 0.0803±0.0010 |
| | | | Case 4 (J) | | | |
| density | 10 | 46.1±68.0 | 44.7 ± 67.4 | 2.1 ± 5.3 | 1.5 ± 2.9 | 2.3 ± 4.6 |
| $\tau$(3889) | 0.0 | (0.0) | 0.030±0.052 | 0.022 ± 0.021 | 0.023 ± 0.022 | 0.023 ± 0.021 |
| abs(He i) | 0.1 | 0.094±0.093 | 0.097 ± 0.094 | (0.0) | 0.084 ± 0.092 | 0.057 ± 0.035 |
| He/H | 0.080 | 0.0793±0.0024 | 0.0793±0.0019 | 0.0764±0.0008 | 0.0777±0.0015 | 0.0772±0.0011 |
| He/H (3) | 0.080 | 0.0793±0.0024 | 0.0793±0.0019 | 0.0787±0.0010 | 0.0800±0.0017 | 0.0796±0.0012 |
| | | | Case 5 (H) | | | |
| density | 10 | 47.1±68.7 | 45.6 ± 68.1 | 1.4 ± 5.2 | 1.0 ± 2.8 | 2.7 ± 6.6 |
| $\tau$(3889) | 0.1 | (0.0) | 0.031±0.058 | 0.220 ± 0.064 | 0.223 ± 0.063 | 0.219 ± 0.064 |
| abs(He i) | 0.1 | 0.095±0.093 | 0.097 ± 0.095 | (0.0) | 0.085 ± 0.091 | 0.058 ± 0.034 |
| He/H | 0.080 | 0.0793±0.0024 | 0.0793±0.0024 | 0.0764±0.0007 | 0.0777±0.0015 | 0.0772±0.0011 |
| He/H (3) | 0.080 | 0.0793±0.0024 | 0.0793±0.0024 | 0.0787±0.0010 | 0.0800±0.0017 | 0.0796±0.0012 |
| | | | Case 6 (G) | | | |
| density | 100 | 111±103 | 108±104 | 2.1± 7.9 | 1.7± 6.2 | 5.9±17.9 |
| $\tau$(3889) | 0.1 | (0.0) | 0.041±0.052 | 0.512 ± 0.096 | 0.503 ± 0.096 | 0.481 ± 0.133 |
| abs(He i) | 0.1 | 0.111±0.104 | 0.115 ± 0.107 | (0.0) | 0.129 ± 0.110 | 0.091 ± 0.036 |
| He/H | 0.080 | 0.0802±0.0031 | 0.0803±0.0032 | 0.0789±0.0008 | 0.0808±0.0018 | 0.0802±0.0011 |
| He/H (3) | 0.080 | 0.0802±0.0031 | 0.0803±0.0032 | 0.0806±0.0010 | 0.0826±0.0019 | 0.0820±0.0013 |

Table 3. Results From Synthetic Spectra with He I $\lambda$7065 5% Low

| Variables | Input | 3 Lines $\tau(\lambda3889) = 0$ | 3 Lines | 5 Lines abs(He i) = 0 | 5 Lines | 6 Lines |
|---|---|---|---|---|---|---|
| | | | Case 1 (B) | | | |
| density | 10 | 34.5±57.0 | 33.9 ± 56.8 | 0.2 ± 1.5 | 0.3 ± 1.6 | 0.2 ± 1.1 |
| $\tau$(3889) | 0.0 | (0.0) | 0.018±0.039 | 0.000 ± 0.001 | 0.000 ± 0.001 | 0.000 ± 0.018 |
| abs(He i) | 0.0 | 0.035±0.059 | 0.037 ± 0.061 | (0.0) | 0.061 ± 0.081 | 0.010 ± 0.018 |
| He/H | 0.080 | 0.0801±0.0018 | 0.0802±0.0018 | 0.0796±0.0007 | 0.0805±0.0014 | 0.0799±0.0008 |
| He/H (3) | 0.080 | 0.0801±0.0018 | 0.0802±0.0018 | 0.0803±0.0010 | 0.0813±0.0015 | 0.0805±0.0010 |
| | | | Case 2 (A) | | | |
| density | 100 | 91.9±92.7 | 90.9 ± 92.5 | 36.3 ± 28.1 | 30.9 ± 26.5 | 30.8 ± 25.5 |
| $\tau$(3889) | 0.0 | (0.0) | 0.028±0.047 | 0.006 ± 0.013 | 0.008 ± 0.015 | 0.007 ± 0.014 |
| abs(He i) | 0.0 | 0.049±0.072 | 0.050 ± 0.074 | (0.0) | 0.073 ± 0.084 | 0.026 ± 0.028 |
| He/H | 0.080 | 0.0811±0.025 | 0.0812±0.0026 | 0.0815±0.0012 | 0.0827±0.0017 | 0.0821±0.0013 |
| He/H (3) | 0.080 | 0.0811±0.025 | 0.0812±0.0026 | 0.0815±0.0013 | 0.0827±0.0018 | 0.0820±0.0015 |
| | | | Case 3 (I) | | | |
| density | 10 | 35.2±57.7 | 34.7 ± 57.5 | 23.4 ± 31.0 | 18.0 ± 27.7 | 15.9 ± 25.1 |
| $\tau$(3889) | 0.1 | (0.0) | 0.020±0.044 | 0.028 ± 0.029 | 0.032 ± 0.029 | 0.032 ± 0.028 |
| abs(He i) | 0.0 | 0.036±0.060 | 0.038 ± 0.062 | (0.0) | 0.041 ± 0.062 | 0.013 ± 0.020 |
| He/H | 0.080 | 0.0802±0.0018 | 0.0802±0.0019 | 0.0796±0.0012 | 0.0804±0.0014 | 0.0802±0.0011 |
| He/H (3) | 0.080 | 0.0802±0.0018 | 0.0802±0.0019 | 0.0798±0.0013 | 0.0806±0.0016 | 0.0802±0.0013 |
| | | | Case 4 (J) | | | |
| density | 10 | 46.1±68.0 | 44.7 ± 67.4 | 0.3 ± 1.6 | 0.4 ± 1.6 | 0.5 ± 1.7 |
| $\tau$(3889) | 0.0 | (0.0) | 0.030±0.052 | 0.000 ± 0.000 | 0.000 ± 0.001 | 0.000 ± 0.001 |
| abs(He i) | 0.1 | 0.094±0.093 | 0.097 ± 0.094 | (0.0) | 0.138 ± 0.112 | 0.094 ± 0.039 |
| He/H | 0.080 | 0.0793±0.0024 | 0.0793±0.0019 | 0.0781±0.0007 | 0.0802±0.0019 | 0.0796±0.0011 |
| He/H (3) | 0.080 | 0.0793±0.0024 | 0.0793±0.0019 | 0.0787±0.0010 | 0.0809±0.0020 | 0.0802±0.0013 |
| | | | Case 5 (H) | | | |
| density | 10 | 47.1±68.7 | 45.6 ± 68.1 | 35.5 ± 35.2 | 21.7 ± 29.4 | 23.3 ± 29.3 |
| $\tau$(3889) | 0.1 | (0.0) | 0.031±0.058 | 0.021 ± 0.027 | 0.030 ± 0.029 | 0.029 ± 0.029 |
| abs(He i) | 0.1 | 0.095±0.093 | 0.097 ± 0.095 | (0.0) | 0.103 ± 0.095 | 0.096 ± 0.038 |
| He/H | 0.080 | 0.0793±0.0024 | 0.0793±0.0024 | 0.0778±0.0012 | 0.0797±0.0018 | 0.0796±0.0015 |
| He/H (3) | 0.080 | 0.0793±0.0024 | 0.0793±0.0024 | 0.0780±0.0014 | 0.0799±0.0020 | 0.0798±0.0017 |
| | | | Case 6 (G) | | | |
| density | 100 | 111±103 | 108±104 | 115±64.7 | 81.4±65.3 | 85.3±65.4 |
| $\tau$(3889) | 0.1 | (0.0) | 0.041±0.052 | 0.048 ± 0.067 | 0.082 ± 0.082 | 0.076 ± 0.079 |
| abs(He i) | 0.1 | 0.111±0.104 | 0.115 ± 0.107 | (0.0) | 0.124 ± 0.106 | 0.106 ± 0.042 |
| He/H | 0.080 | 0.0802±0.0031 | 0.0803±0.0032 | 0.0782±0.0018 | 0.0809±0.0027 | 0.0805±0.0023 |
| He/H (3) | 0.080 | 0.0802±0.0031 | 0.0803±0.0032 | 0.0783±0.0019 | 0.0809±0.0028 | 0.0806±0.0024 |

## A. Monte Carlo Estimates of Reddening and Underlying Balmer Absorption

Here we would like to describe the Monte Carlo procedure we use for determining the corrections for reddening and underlying stellar absorption in the Hydrogen lines. Beginning with an observed line flux $F(\lambda)$, and an equivalent width $W(\lambda)$, we can parameterize the correction for underlying stellar absorption as

$$X_A(\lambda) = F(\lambda)(\frac{W(\lambda) + a_{HI})}{W(\lambda)}) \tag{A1}$$

The parameter $a_{HI}$ is expected to be relatively insensitive to wavelength because all of the Balmer lines should be saturated in the stars which are producing the underlying continuum. As described in section 2, the reddening correction is applied to determine the intrinsic line intensity $I(\lambda)$ relative to $H\beta$

$$X_R(\lambda) = \frac{I(\lambda)}{I(H\beta)} = \frac{X_A(\lambda)}{X_A(H\beta)} 10^{f(\lambda)C(H\beta)} \tag{A2}$$

We assume the intrinsic Balmer line ratios calculated by Hummer & Storey (1987), and we use the reddening function, $f(\lambda)$, normalized at H$\beta$, from the Galactic reddening law of Seaton (1979), as parameterized by Howarth (1983), assuming a value of $\mathrm{R} \equiv \mathrm{A_V/E_{B-V}} = 3.2$. By comparing $X_R(\lambda)$ to theoretical values, $X_T(\lambda)$, we determine the parameters $a_{HI}$ and $C(H\beta)$ self consistently, and run a Monte Carlo over the input data to test the robustness of the solution and to determine the systematic uncertainty associated with these corrections.

For definiteness, we list here the theoretical ratios we use:

$$\begin{aligned} X_T(6563) &= 0.3862(\log T_4)^2 - 0.4817 \log T_4 + 2.86 \\ X_T(4340) &= -0.01655(\log T_4)^2 - 0.02824 \log T_4 + 0.468 \\ X_T(4101) &= -0.01655(\log T_4)^2 - 0.02159 \log T_4 + 0.259 \end{aligned} \tag{A3}$$

where the temperature is $T_4 = T/10^4\mathrm{K}$. The values for $f(\lambda)$ we take are

$$f(6563) = -0.329 \qquad f(4340) = 0.137 \qquad f(4101) = 0.193 \tag{A4}$$

We begin therefore with four input fluxes $F(\lambda)$ along with their associated observational (statistical) uncertainties and four equivalent widths (and their observational uncertainties). In addition, the theoretical ratios are temperature dependent, so we must add the temperature and its uncertainty as an additional observational input. From these, the ratios, $X_R(\lambda)$ for $H\alpha, H\gamma$, and $H\delta$ are obtained. The $\chi^2$ statistic is defined by

$$\chi^2 = \sum_\lambda \frac{(X_R^2(\lambda) - X_T^2(\lambda))}{\sigma_{X_R}^2(\lambda)} \tag{A5}$$

where $\sigma_{X_R}(\lambda)$ is the derived uncertainty in $X_R$. The minimization of $\chi^2$, allows us to determine the values of $a_{HI}$ and $C(H\beta)$. The uncertainties in the two outputs are determined by varying the solution so that $\chi^2(a \pm \sigma_a) - \chi^2(a) = 1$. $\sigma_{C(H\beta)}$ is similarly determined.

As we indicated above, we further test this solution and its robustness by running a Monte Carlo on the input data. This also allows us to better determine the systematic uncertainty in the output parameters $a_{HI}$ and $C(H\beta)$. The data for the Monte Carlo are generated from the input data, $F(\lambda), W(\lambda)$ and temperature and the uncertainties in these quantities. A Gaussian distribution of input values centered on the observed values with a spread determined by their observational uncertainties. A new set of data is then randomly generated by picking input values from these Gaussian distributions. Consequently, after running the $\chi^2$ minimization procedure, new values for the output parameters $a_{HI}$ and $C(H\beta)$ are found. Our Monte Carlo produces 1000 randomly generated data sets from which we can produce a distribution of solutions for $a_{HI}$ and $C(H\beta)$. One would expect that the mean of the solutions for $a_{HI}$ and $C(H\beta)$ tracks the original solution based on the actual observational data. The spread in these allows us to test the systematic uncertainty associated with these quantities.

## B. Monte Carlo Estimates of Reddening and Underlying Balmer Absorption in Real Observations

Here we provide examples of deriving reddening and underlying stellar absorption from emission line spectra. We take as a examples, the observations of SBS1159+545, SBS1415+437, and SBS1420+544 as reported in IT98. These three spectra are all reported with very high accuracy; the brightest lines are reported with errors of less than one percent. Since the emission line equivalent widths for all of the Balmer lines are required as input and since only the emission line equivalent width for H$\beta$ is reported, we have had to estimate these from the relative line strengths and the spectra shown in figures. The fractional uncertainties in the equivalent widths were assumed to be twice as large as the fractional uncertainties reported in the relative intensities.

We used the values reported in IT98 and calculated C(H$\beta$) and $a_{HI}$ for the three targets. Our results are shown in Figure B-1. Here we display the originally observed Balmer line ratios, the corrected ratios reported in IT98 and our own solutions. There are two important points to note. First note that the IT98 corrected values for the H$\gamma$/H$\beta$ and H$\delta$/H$\beta$ ratios are several $\sigma$ away from the theoretical values. In the case of SBS 1159+545, this is because these ratios were already higher than the theoretical ratios, and correcting for reddening and underlying absorption only increases the ratios. In the other two cases, the original ratios were very close to the theoretical ratios, but correcting the H$\alpha$/H$\beta$ ratio for reddening has caused these ratios to exceed their theoretical ratios. Since the deviations from the theoretical line ratios are large (yielding generally high values of the $\chi^2$), we conclude that the uncertainties in the reported emission lines are underestimated.

The second point to note in Figure B-1 is the difference between our solutions are those of IT98. In all three cases, the IT98 solution yields very good agreement with theory in the H$\alpha$/H$\beta$ ratio (better than ours) but not as good in the other lines. It would appear that the weighting scheme used by IT98 favors this line ratio more than would be called for by the relative errors in the line ratios.

### C. Monte Carlo Estimates of Self-Consistent Helium Line Ratios

For $^4$He, we follow an analogous procedure to that described above. We again start with a set of observed quantities: line intensities $I(\lambda)$ which include the reddening correction previously determined and its associated uncertainty which also includes the uncertainty in $C(H\beta)$; the equivalent width $W(\lambda)$; and temperature $t$. The Helium line intensities are scaled to $H\beta$ and the singly ionized helium abundance is given by

$$y^+(\lambda) = \frac{I(\lambda)}{I(H\beta)} \frac{E(H\beta)}{E(\lambda)} (\frac{W(\lambda) + a_{He\ i)}}{W(\lambda)}) \frac{1}{(1+\gamma)} \frac{1}{f(\tau)} \tag{C1}$$

where $E(\lambda)/E(H\beta)$ is the theoretical emissivity scaled to $H\beta$. The expression (C1), also contains a correction factor for underlying stellar absorption, parameterized now by $a_{HeI}$, a density dependent collisional correction factor, $(1+\gamma)^{-1}$, and a florescence correction which depends on the optical depth $\tau$. Thus $y^+$ implicitly depends on three unknowns, the electron density, $n$, $a_{HeI}$, and $\tau$.

To be definite, we list here the necessary components in expression (C1). The theoretical emissivities scaled to $H\beta$ are taken from Smits (1996):

$$\begin{aligned}
E(H\beta)/E(3889) &= 0.9072T^{-0.1715} \\
E(H\beta)/E(4026) &= 4.3166T^{0.0847} \\
E(H\beta)/E(4471) &= 2.0094T^{0.1259} \\
E(H\beta)/E(5876) &= 0.7355T^{0.2298} \\
E(H\beta)/E(6678) &= 2.5861T^{0.2475} \\
E(H\beta)/E(7065) &= 4.3588T^{-0.3456}
\end{aligned} \tag{C2}$$

Our expressions for the collisional correction $\gamma$, are taken from Kingdon & Ferland (1995). We list them here for completeness. They are:

$$\begin{aligned}
\gamma(3889) &= (9.34T_4^{-0.92}e^{-3.699/T_4} + 1.64T_4^{-0.79}e^{-4.379/T_4} + 0.83T_4^{-0.40}e^{-4.545/T_4} \\
&\quad +0.51T_4^{-1.05}e^{-4.818/T_4} + 0.39T_4^{-0.36}e^{-4.900/T_4})/D \\
\gamma(4026) &= (6.92T_4^{-0.45}e^{-4.900/T_4})/D \\
\gamma(4471) &= (6.95T_4^{0.15}e^{-4.545/T_4} + 0.22T_4^{-0.55}e^{-4.884/T_4} + 0.98T_4^{-0.45}e^{-4.901/T_4})/D \\
\gamma(5876) &= (6.78T_4^{0.07}e^{-3.776/T_4} + 1.67T_4^{-0.15}e^{-4.545/T_4} + 0.60T_4^{-0.34}e^{-4.901/T_4})/D \\
\gamma(6678) &= (3.15T_4^{-0.54}e^{-3.776/T_4} + 0.51T_4^{-0.51}e^{-4.545/T_4} + 0.20T_4^{-0.66}e^{-4.901/T_4})/D \\
\gamma(7065) &= (38.09T_4^{-1.09}e^{-3.364/T_4} + 2.80T_4^{-1.06}e^{-3.699/T_4})/D
\end{aligned} \tag{C3}$$

where $D = 1 + 3130n^{-1}T_4^{-0.50}$. The corrections for florescence are given in terms of the optical depth for the He I $\lambda\lambda$3389 line. We use the IT98 fit of the Robbins (1968) enhancement factors:

$$f(3889) = 2.25 \times 10^{-7}\tau^4 - 3.87 \times 10^{-5}\tau^3 + 2.39 \times 10^{-3}\tau^2 - 0.069\tau + 1$$

$$
\begin{aligned}
f(4026) &= 1 \\
f(4471) &= 1 + 0.001\tau \\
f(5876) &= 1 + 0.0049\tau \\
f(6678) &= 1 \\
f(7065) &= 1 + 0.4\tau^{0.55}
\end{aligned} \tag{C4}
$$

$f(4026)$ is not given by IT98, but is assumed to be 1 because it is a singlet line (as is the case for $\lambda$6678).

Once the individual values for $y^+(\lambda)$ are determined, we can begin the process for self-consistently determining the physical parameters. As described in the text, we may wish to consider 3,5, or 6 different $^4$He emission lines. Depending on the number of lines used, we next determine the average helium abundance. $\bar{y}$,

$$\bar{y} = \sum_{\lambda} \frac{y^+(\lambda)}{\sigma(\lambda)^2} / \sum_{\lambda} \frac{1}{\sigma(\lambda)^2} \tag{C5}$$

This is a weighted average, where the uncertainty $\sigma(\lambda)$ is found by propagating the uncertainties in the observational quantities stemming from the observed line fluxes (which already contains the uncertainty due to C(H$\beta$), the equivalent widths, and input temperature. Since the average, $\bar{y}$, depends on the parameters, $n, \tau$ and $a_{HeI}$, we must make an initial estimate for these.

From $\bar{y}$, we can define a $\chi^2$ as the deviation of the individual He abundances $y^+(\lambda)$ from the average,

$$\chi^2 = \sum_{\lambda} \frac{(y^+(\lambda) - \bar{y})^2}{\sigma(\lambda)^2} \tag{C6}$$

We then minimize $\chi^2$, to determine $n, a_{HeI}$, and $\tau$. Uncertainties in the output parameters are determined as in the case for $a_{HI}$ and $C(H\beta)$, that is by varying the outputs until $\Delta\chi^2 = 1$. Propagation in the latter uncertainties give us a reasonable handle on the systematic uncertainties in our final result for $y^+$.

This procedure differs somewhat from that proposed by IT98, in that the $\chi^2$ above (C6) is a straight weighted average, whereas IT98 minimize the differences between ratios of He abundances from pairs of He I lines (referenced to one wavelength, typically 4471). When the reference line is particularly sensitive to a systematic effect such as underlying stellar absorption, the uncertainty propagates to all lines this way. In our case, the individual uncertainties in the line strengths are kept separate.

Finally, as in the case for the hydrogen lines, we have performed a Monte-Carlo simulation of the data to test the robustness of the solution for $n, a_{HeI}$, and $\tau$ from the $\chi^2$ minimization and the true uncertainty in these quantities. As before, starting with the observational inputs and their stated uncertainties, we have generated a data set which is Gaussian distributed for the 6 observed He emission lines (plus the temperature). From each distribution, we randomly select a set of input values and run the $\chi^2$ minimization. The selection of data is repeated 1000 times. We thus obtain a distribution of solutions for $n, a_{HeI}$, and $\tau$, and we compare the mean and dispersion of these distributions with the initial solution for these quantities.

## REFERENCES

Almog, Y., & Netzer, H. 1989, MNRAS, 238, 57

Auer, L. H., & Mihalas, D. 1972, ApJS, 24, 193

Benjamin, R. A., Skillman, E. D., & Smits, D. P., 1999, ApJ, 514, 307

Berrington, J.A., Burke, P.G., Freitas, L.C.G., & Kingston, A.E. 1985, J. Phys. B, 18, 4135

Berrington, J.A. & Kingston, A.E. 1987, J. Phys. B, 20, 6631

Brocklehurst, M. 1971, MNRAS, 153, 471

Brocklehurst, M. 1972, MNRAS, 157, 211

Burles, S. & Tytler, D. 1998a, ApJ, 499, 699

Burles, S. & Tytler, D. 1998b, ApJ, 507, 732

Cardelli, J. A., Clayton, G. C., & Mathis, J. S. 1989, ApJ, 345, 245

Davidson, K. & Kinman, T. D. 1985, ApJS, 58, 321

De Robertis, M., Dufour, R. J., & Hunt, R. 1987, JRASC, 81, 195

Dinerstein, H. L., & Shields, G. A. 1986, ApJ, 311, 45

Fields, B.D. & Olive, K.A. 1998, ApJ, 506, 177

Filippenko, A.V. 1982, PASP, 94, 715

Garnett, D. R. 1992, AJ, 103, 1330

González-Delgado, R.M., Pérez, E., Tenorio-Tagle, G, Vilchez, J.M., et al. 1994, ApJ, 437, 239

Hogan, C. J., Olive, K. A., Scully, S. T. 1997, ApJL, 489, 119

Hummer, D. G. & Storey, P. J. 1987, MNRAS, 224, 801

Howarth, I.D. 1983, MNRAS, 203, 301

Izotov, Y. I., Chaffee, F. H., Foltz, C. B., Green, R. F., Guseva, N. G., & Thuan, T.X. 1999, ApJ, 527, 757 (I99)

Izotov, Y. I., Thuan, T. X., & Lipovetsky, V. A. 1994, ApJ, 435, 647 (ITL94)

Izotov, Y. I., Thuan, T. X., & Lipovetsky, V. A. 1997, ApJS, 108, 1 (ITL97)

Izotov, Y. I., & Thuan, T. X. 1998a, ApJ, 497, 227

Izotov, Y. I., & Thuan, T. X. 1998b, ApJ, 500, 188 (IT98)

Kingdon, J., & Ferland, G. 1995, ApJ, 442, 714

Kinman, T.D. & Davidson, K. 1981, ApJ, 243, 127

Kono, A., & Hattori, S. 1984, Phys. Rev. A, 29, 2981

Kunth, D., & Sargent, W. L. W. 1983, ApJ, 273, 81

Lennon, D. J., Dufton, P. L., & Fitzsimmons, A. 1992, A&AS, 94, 569

Lennon, D. J., Dufton, P. L., & Fitzsimmons, A. 1993, A&AS, 97, 559

Levshakov, S., Tytler, D., & Burles, S. 1998, astro-ph/9812114

Mathis, J.S. 1982, ApJ, 261, 195

Oke, J. B. 1990, AJ, 99, 1621

Olive, K. A., Skillman, E. D., & Steigman, G. 1997, ApJ, 483, 788

Olive, K., & Steigman, G. 1995, ApJS, 97, 49

Olive, K. A., Steigman, G. & Walker, T.P. 2000, Phys Rep, in press, astro-ph/9905320

Olofsson, K. 1995, A&AS, 111, 57

Osterbrock, D. E. 1989, *Astrophysics of Gaseous Nebulae and Active Galactic Nuclei*, University Science Books.

Pagel, B. E. J., & Simonson, E. A. 1989, Rev. Mex. Astr. Astrofis., 18, 153

Pagel, B. E. J., Simonson, E. A., Terlevich, R. J., & Edmunds, M. G. 1992, MNRAS, 255, 325 (PSTE)

Peimbert, M., Peimbert, A., & Ruiz, M. T. 2000, ApJ, in press, Astro-ph 000315

Peimbert, M., & Torres-Peimbert, S. 1974, ApJ, 193, 327

Peimbert, M., & Torres-Peimbert, S. 1976, ApJ, 203, 581

Proga, D., Mikolajewska, J., & Kenyon S.J. 1994, MNRAS, 268, 213

Robbins, R.R. 1968, ApJ, 151, 511

Robbins, R.R., & Bernat A.P. 1973, Mem. Soc. R. Sci. Liège, 6(5), 263

Ryan, S.G., Beers, T.C., Olive, K.A., Fields, B.D., & Norris, J.E. 2000, ApJ, 530, L57

Ryan, S.G., Norris, J.E., & Beers, T.C. 1999, ApJ, 523, 654

Sasselov, D. & Goldwirth, D.S. 1995, ApJ, 444, L5

Sawey, P. M. J., & Berrington, K. A. 1993, *Atomic Data Nucl. Data Tables*, 55, 81

Seaton, M. J. 1979, MNRAS, 187, 73p

Shaw, R. A., & Dufour, R. J. 1995, PASP, 107, 896 (SD95)

Shields, G.A., & Searle, L. 1978, ApJ, 222, 821

Skillman, E. 1985, ApJ, 290, 449

Skillman, E. D., & Kennicutt, R. C., Jr. 1993, ApJ, 411, 655

Skillman, E. D., Terlevich, R. J., Kennicutt, R. C., Garnett, D. R., & Terlevich, E. 1994, ApJ, 431, 172

Skillman, E. D., Terlevich, E., & Terlevich, R. 1998, Space Science Reviews, 84, 105

Smits, D.P. 1996, MNRAS, 251, 316

Stasińska, G. 1990, A&AS, 83, 501

Stasińska, G., & Schaerer, D. 1999, A&A, 351, 72

Steigman, G., Viegas, S.M., & Gruenwald, R. 1997, ApJ, 490, 187

Tytler, D., Burles, S., Lu, L., Fan, X.-M., Wolfe, A., & Savage, B.D. 1999, AJ, 117, 63

Viegas, S.M., Gruenwald, R., & Steigman, G. 2000, ApJ, 531, 813

Vílchez, J. M. & Pagel, B. E. J. 1988, MNRAS, 231, 257

Webb, J. K., Carswell, R. F., Lanzetta, K. M., Ferlet, R., Lemoine, M., Vidal-Madjar, A., & Bowen, D. V. 1997, Nature, 388, 250

**Figure Captions**

**Figure 1:** A comparison of the observed and corrected hydrogen Balmer emission line ratios for three synthetic cases (with no errors). The open circles show the deviations of the original synthesized spectra from the theoretical ratios in terms of the synthesized uncertainties (assumed to be 2% for all lines). The filled circles show the corrected values in the same manner. Note that the corrections for reddening and underlying absorption all have the same sense for all three line ratios, i.e., the H$\alpha$/H$\beta$ line ratio increases for increased reddening and underlying absorption and the higher order Balmer line ratios all decrease for both effects. This covariance results in decreased diagnostic power as shown in Figure 2.

**Figure 2:** The results of Monte Carlo simulations of solutions for the reddening and underlying absorption from hydrogen Balmer emission line ratios for three synthetic cases. Each small point is the solution derived from a different realization of the same input spectrum (with 2% errors in both emission line flux and equivalent width). The original input spectra had reddening with C(H$\beta$) = 0.1 and $a_{HI} = 2$ Å. The large filled point with error bars shows the mean result with $1\sigma$ errors derived from the dispersion in the solutions. Note that the covariance of the two parameters leads to error ellipses. The Monte Carlo simulations find the correct solutions, but the error bars appropriate to these solutions are about twice the size of the errors inferred from single $\chi^2$ minimizations. Note that the covariance of the two parameters leads to error ellipses. Note also that, given the input assumptions, that the constraints on the underlying absorption are stronger in absolute terms for the lower emission line equivalent width cases.

**Figure 3:** Graphs showing the IT98 fits to the florescence enhancement figures reported in Robbins (1968). The important point to note is that regime of the calculations is mostly at far larger values of $\tau(3889)$ than is relevant for work with giant extragalactic HII regions. More detailed work concentrating on the relevant regime is needed.

**Figure 4:** Histograms showing the effects on helium emission lines due to changes in physical parameters. The baseline model is a photoionized gas at 15,000 K with a density of 10 cm$^{-3}$, a negligible optical depth in the $\lambda$3889 line, and no underlying absorption in the helium lines (the underlying spectrum has a $\lambda^{-2}$ slope and the equivalent width of the H$\beta$ emission line is 100 Å). The top panel shows that the helium lines are very insensitive to variations in temperature, with differences of order 1% or less for a 500 K variations. The second panel shows that all of the helium lines are sensitive to an increase in density, but that the $\lambda$7065 line is far more sensitive than the other lines. The third panel shows that only the $\lambda$3889 and $\lambda$7065 lines have significant sensitivity to optical depth effects. The bottom panel shows that all lines are very sensitive to small increases in the underlying absorption.

**Figure 5:** Results of modeling of 6 synthetic He I line observations. The four panels show the results of

a density = 10, $a_{HeI} = 0$, and $\tau(3889) = 0$ model. The solid lines show the input values (e.g., He/H = 0.080) for the original calculated spectrum. The solid circles (with error bars) show the results of the $\chi^2$ minimization solution (with calculated errors) for the original synthetic input spectrum. The small points show the results of Monte Carlo realizations of the original input spectrum. The solid squares (with error bars) show the means and dispersions of the output values for the $\chi^2$ minimization solutions of the Monte Carlo realizations.

**Figure 6:** Similar plot to Figure 5 except that the density = 100 as opposed to 10 as in Figure 5.

**Figure 7:** Similar plot to Figure 6 except that the underlying absorption is 0.1 Åand $\tau(3889) = 0.1$.

**Figure 8:** Similar plot to Figure 6 except that I($\lambda$3889) and EW($\lambda$3889) are artificially decreased by 10%.

**Figure 9:** Similar plot to Figure 6 except that I($\lambda$7065) and EW($\lambda$7065) are artificially decreased by 5%.

**Figure 10:** Similar plot to Figure 7 except that I($\lambda$7065) and EW($\lambda$7065) are artificially decreased by 5%.

**Figure B-1:** A comparison of the observed and corrected hydrogen Balmer emission line ratios for three blue compact galaxies from the sample of IT98. The open circles show the deviations of the original observations from the theoretical ratios in terms of the uncertainties in the final reported corrected values (the H$\alpha$/H$\beta$ ratios for SBS 1415+437 and SBS 1420+544 are off scale at + 33 $\sigma$ and + 25 $\sigma$ respectively). The filled circles show the corrected values in the same manner. Note that in all three cases the corrected H$\gamma$/H$\beta$ and H$\delta$/H$\beta$ ratios are several $\sigma$ away from the theoretical values. In the case of SBS 1159+545, this is because these ratios were already higher than the theoretical ratios, and correcting for reddening and underlying absorption only increases the ratios. In the other two cases, the original ratios were very close to the theoretical ratios, but correcting the H$\alpha$/H$\beta$ ratio for reddening has caused these ratios to exceed their theoretical ratios. Since the deviations from the theoretical line ratios are large, we conclude that the uncertainties in the reported emission lines are underestimated.

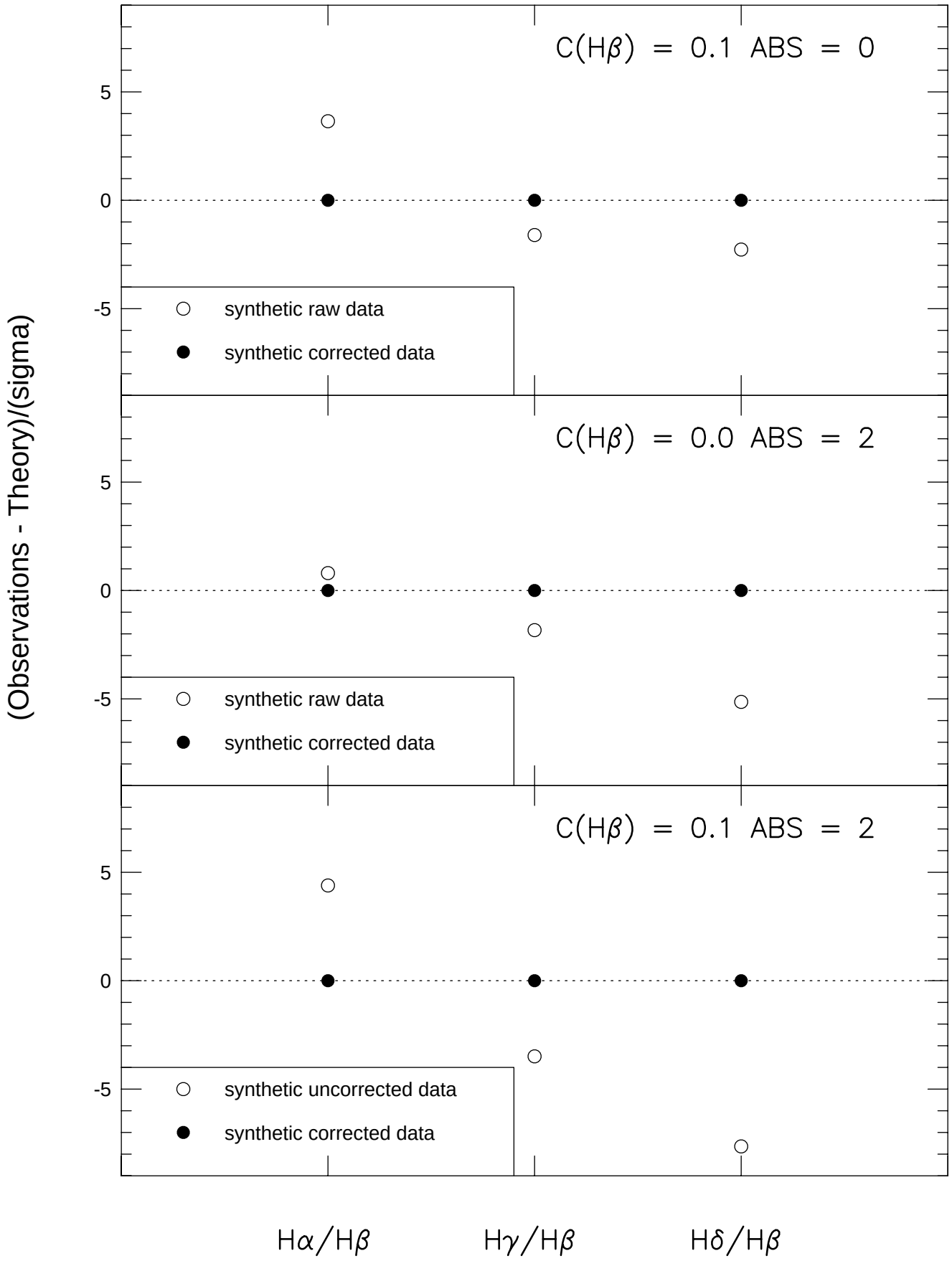
C(Hβ) = 0.1 ABS = 0
C(Hβ) = 0.0 ABS = 2
C(Hβ) = 0.1 ABS = 2
synthetic raw data
synthetic corrected data
synthetic uncorrected data
synthetic corrected data
5
0
-5
(Observations - Theory)/(sigma)
Hα/Hβ
Hγ/Hβ
Hδ/Hβ

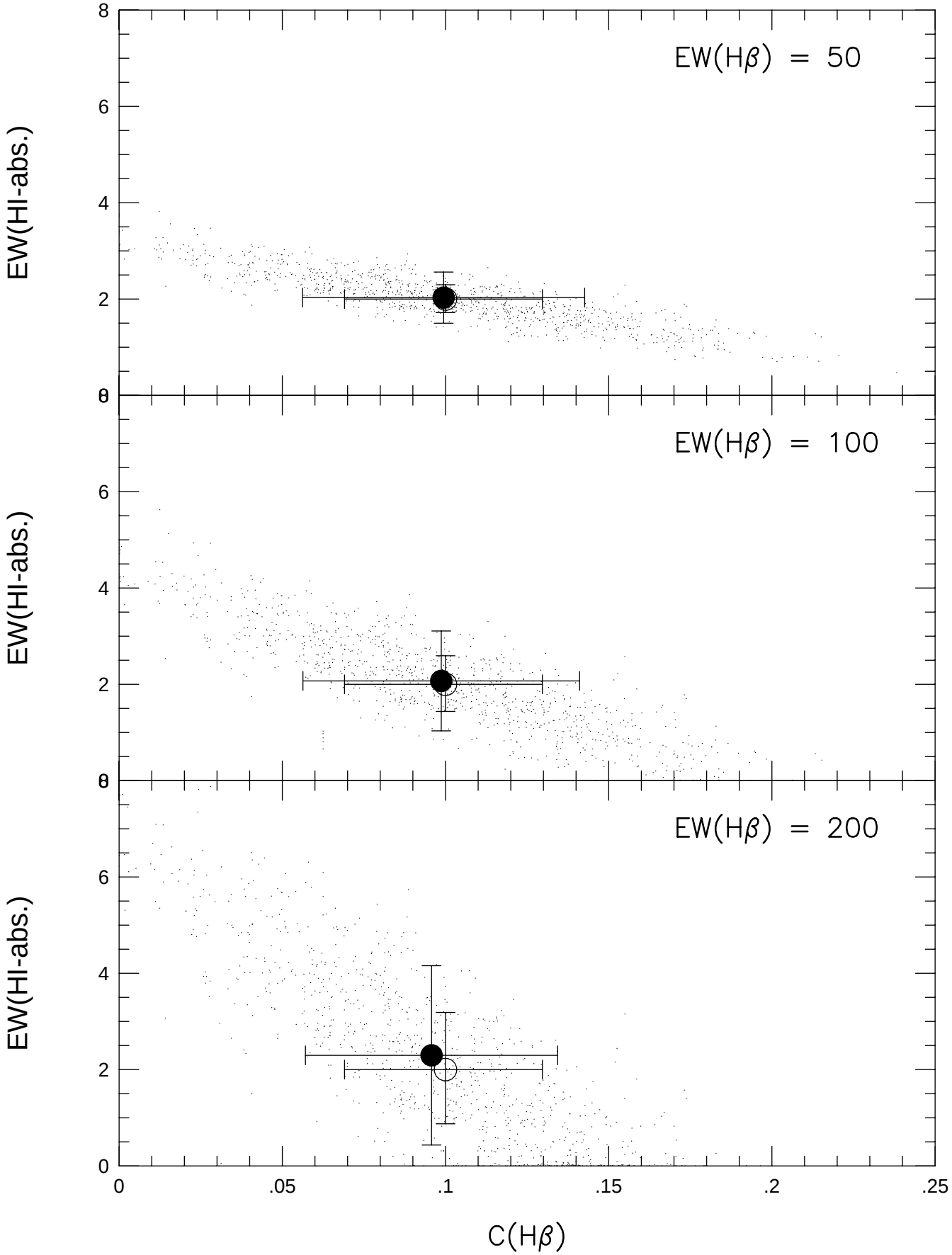
EW(Hβ) = 50
EW(Hβ) = 100
EW(Hβ) = 200
EW(HI-abs.)
EW(HI-abs.)
EW(HI-abs.)
C(Hβ)
0
2
4
6
8
0
.05
.1
.15
.2
.25

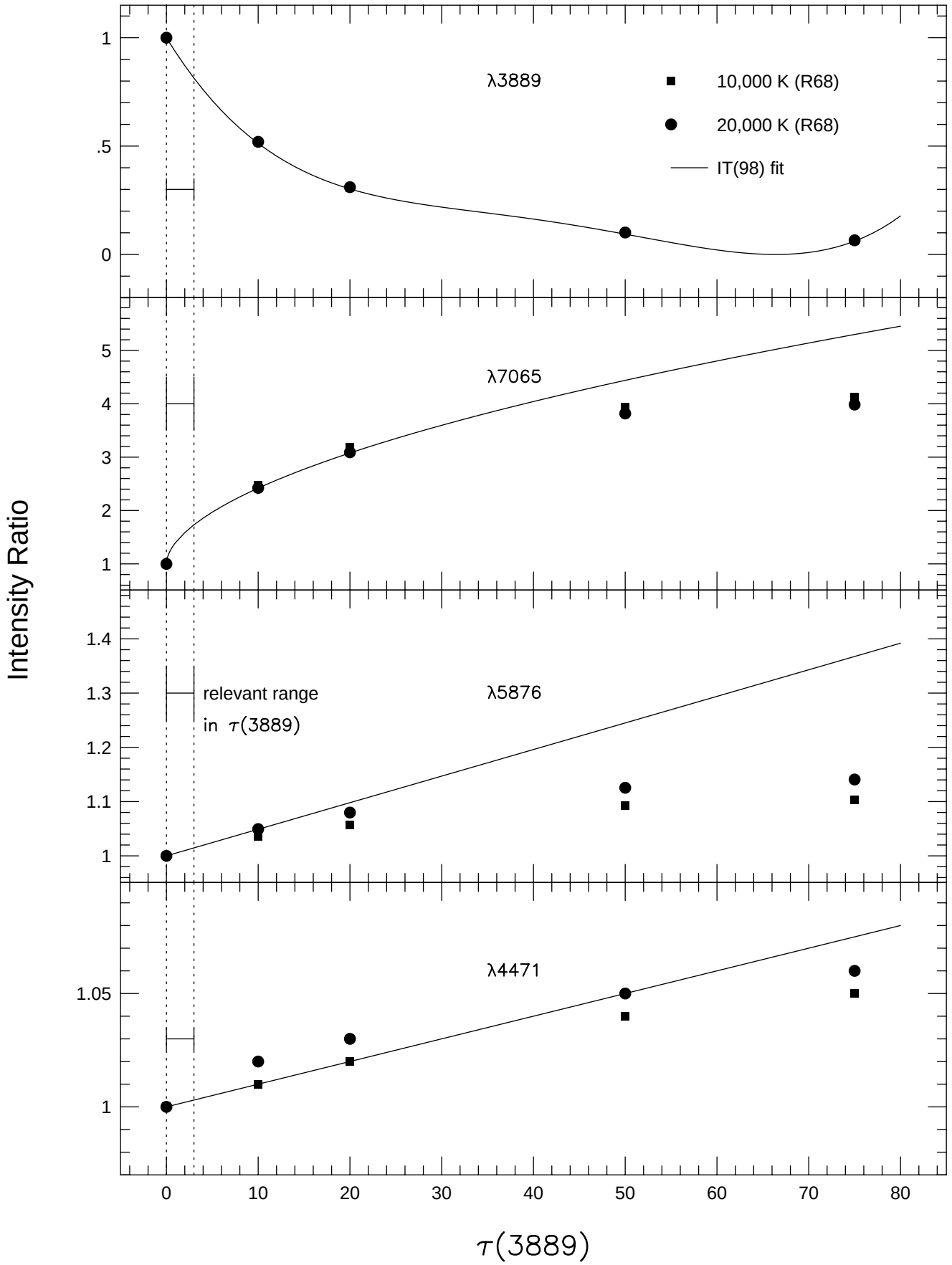
λ3889
10,000 K (R68)
20,000 K (R68)
IT(98) fit
λ7065
λ5876
relevant range
in τ(3889)
λ4471
Intensity Ratio
τ(3889)

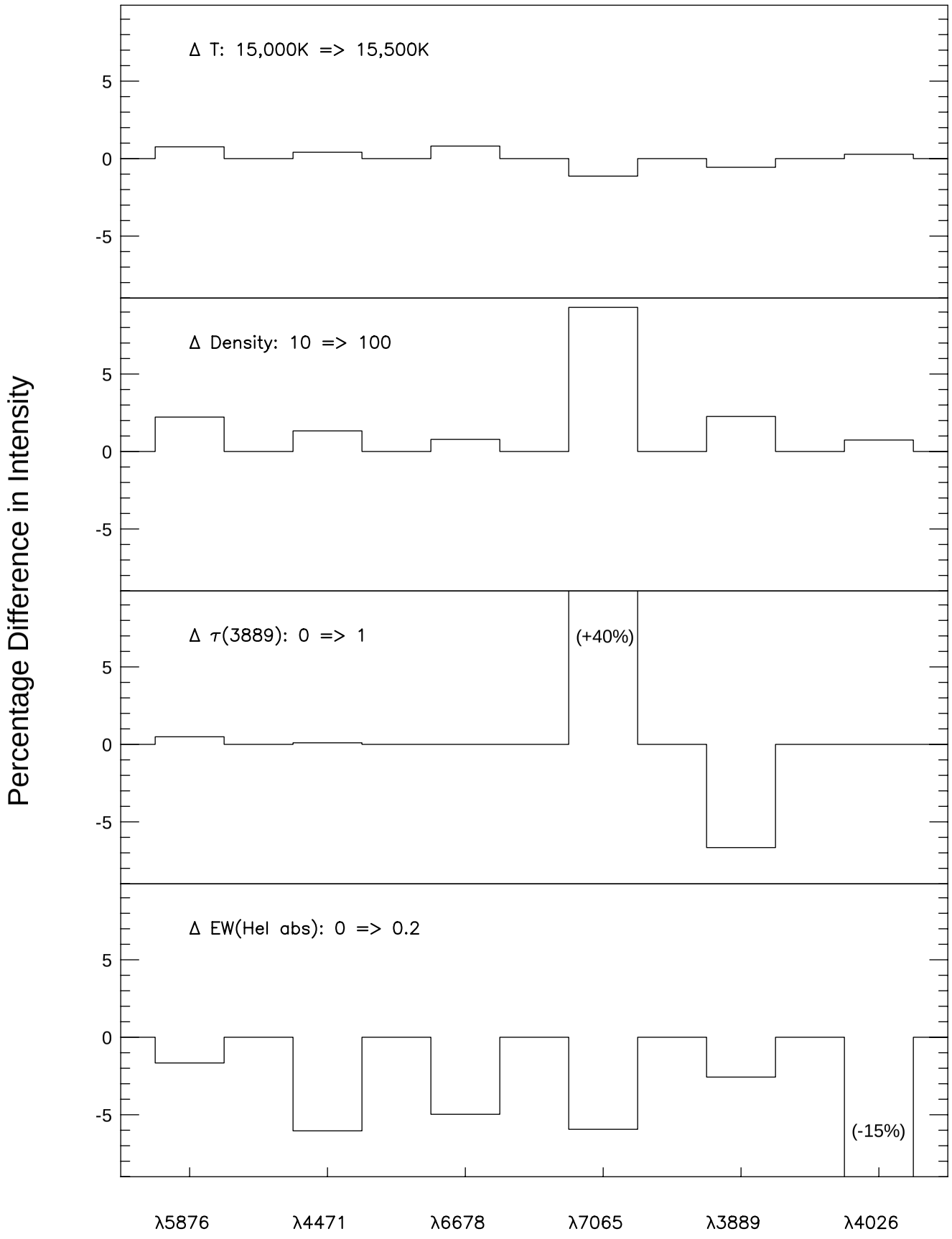
Δ T: 15,000K => 15,500K
Δ Density: 10 => 100
Δ τ(3889): 0 => 1
(+40%)
Δ EW(HeI abs): 0 => 0.2
(-15%)
5
0
-5
Percentage Difference in Intensity
λ5876
λ4471
λ6678
λ7065
λ3889
λ4026

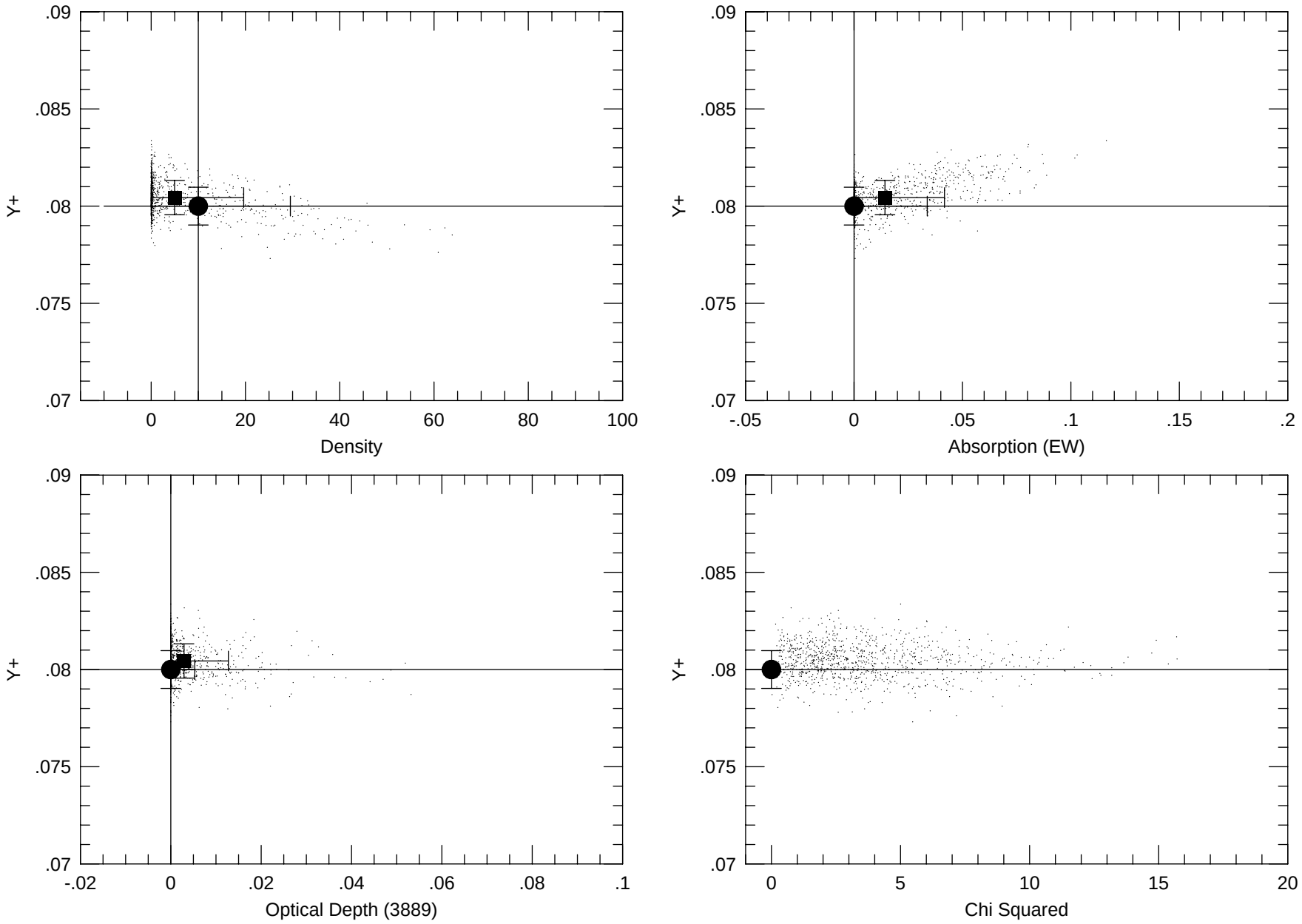
Synthetic Data (T = 1.8, EW(HB) = 100)
Y+
.09
.085
.08
.075
.07
0
20
40
60
80
100
Density
-.05
0
.05
.1
.15
.2
Absorption (EW)
-.02
0
.02
.04
.06
.08
.1
Optical Depth (3889)
0
5
10
15
20
Chi Squared

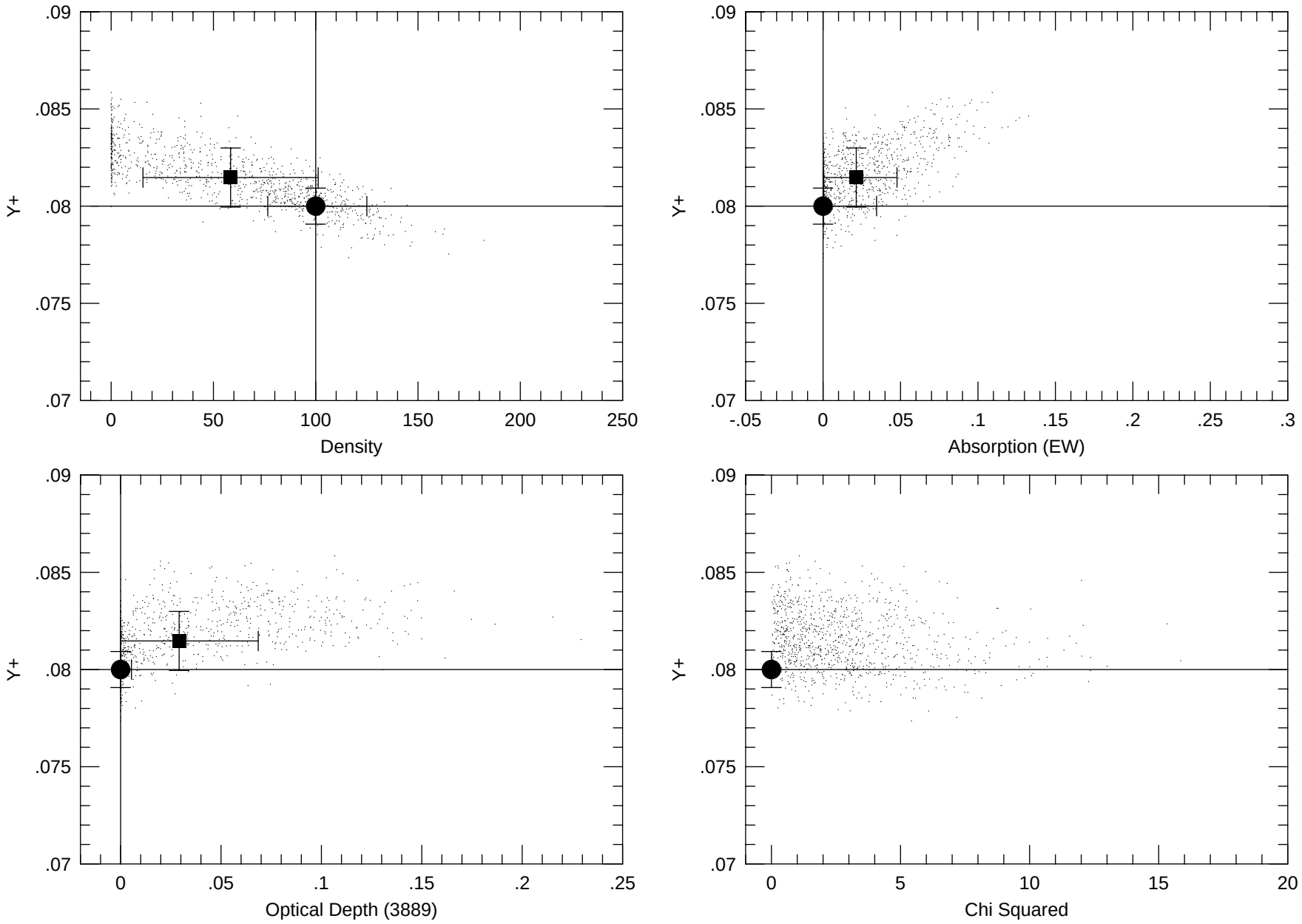
Synthetic Data (T = 1.8, EW(HB) = 100)
Y+
.09
.085
.08
.075
.07
0
50
100
150
200
250
Density
-.05
.05
.1
.15
.2
.25
.3
Absorption (EW)
.2
.25
Optical Depth (3889)
5
10
15
20
Chi Squared

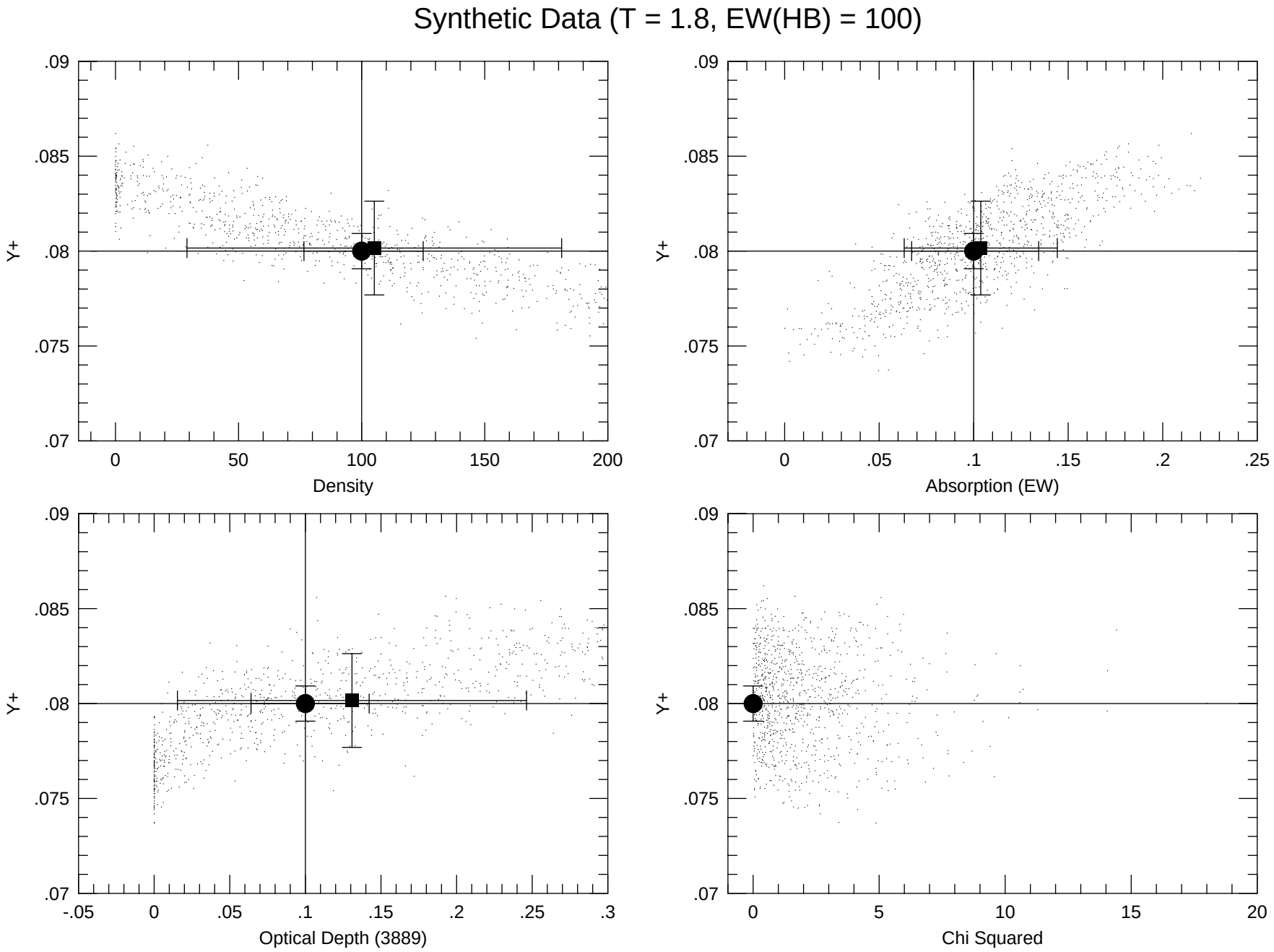
Synthetic Data (T = 1.8, EW(HB) = 100)
Y+
.09
.085
.08
.075
.07
0
50
100
150
200
Density
0
.05
.1
.15
.2
.25
Absorption (EW)
-.05
0
.05
.1
.15
.2
.25
.3
Optical Depth (3889)
0
5
10
15
20
Chi Squared

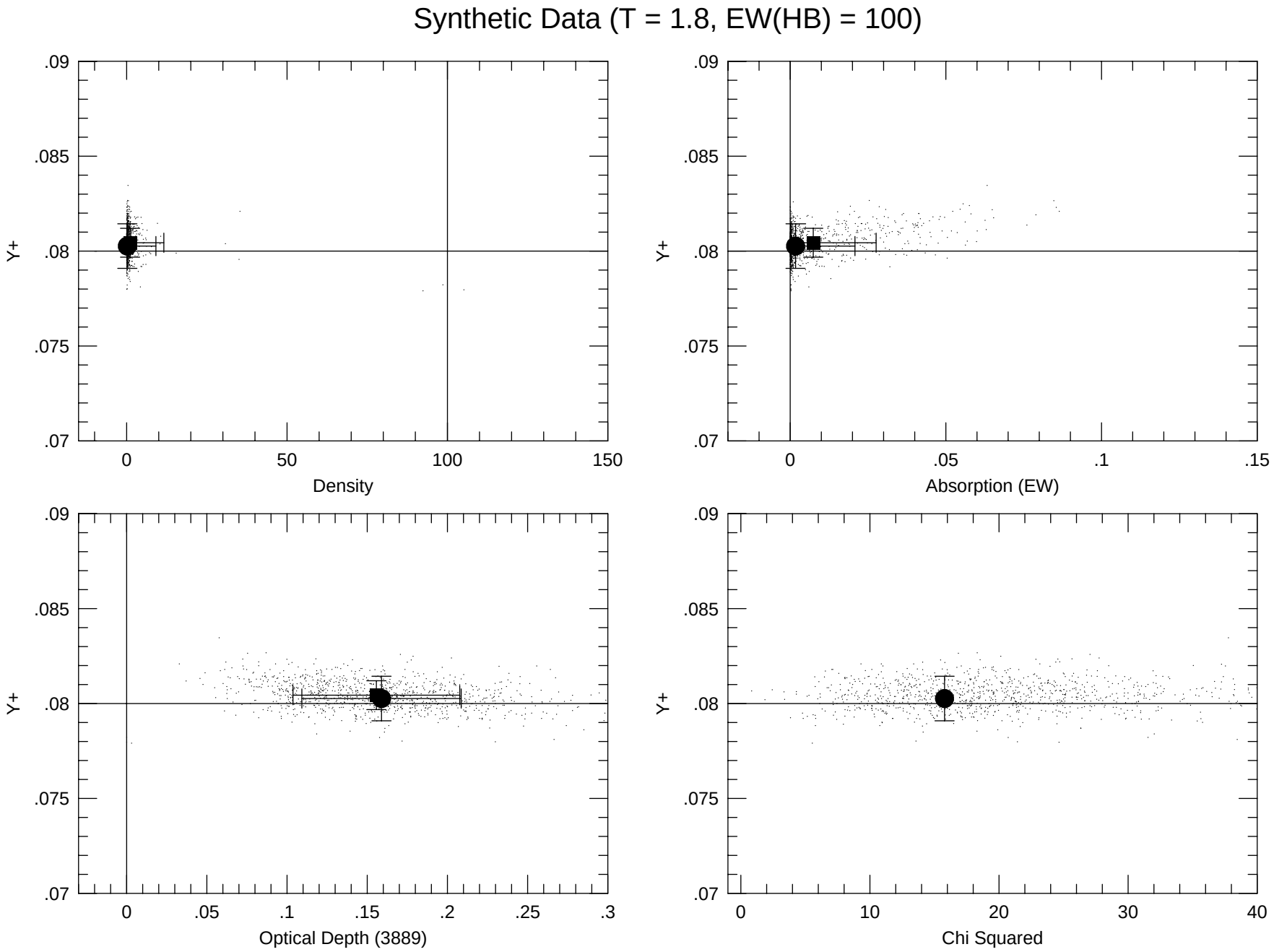
Synthetic Data (T = 1.8, EW(HB) = 100)
Y+
.09
.085
.08
.075
.07
0
50
100
150
Density
0
.05
.1
.15
Absorption (EW)
0
.05
.1
.15
.2
.25
.3
Optical Depth (3889)
0
10
20
30
40
Chi Squared

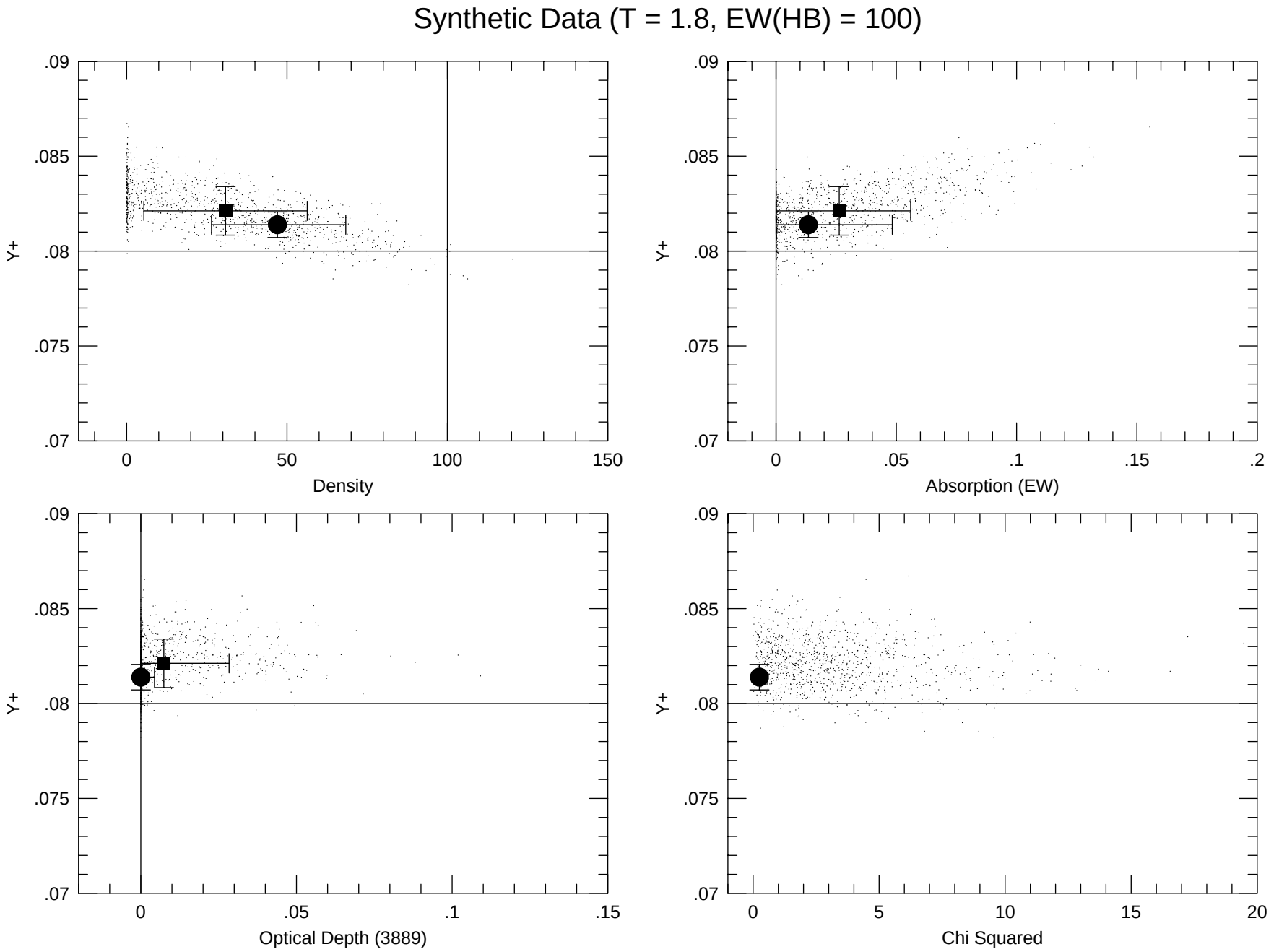
Synthetic Data (T = 1.8, EW(HB) = 100)
.09
.085
.08
.075
.07
Y+
0
50
100
150
Density
0
.05
.1
.15
.2
Absorption (EW)
0
.05
.1
.15
Optical Depth (3889)
0
5
10
15
20
Chi Squared

# Synthetic Data (T = 1.8, EW(HB) = 100)

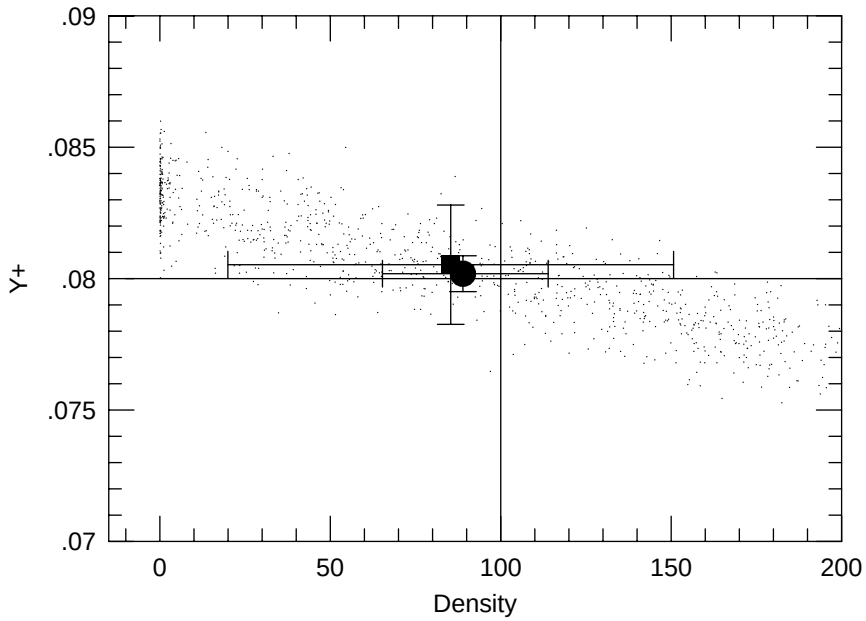


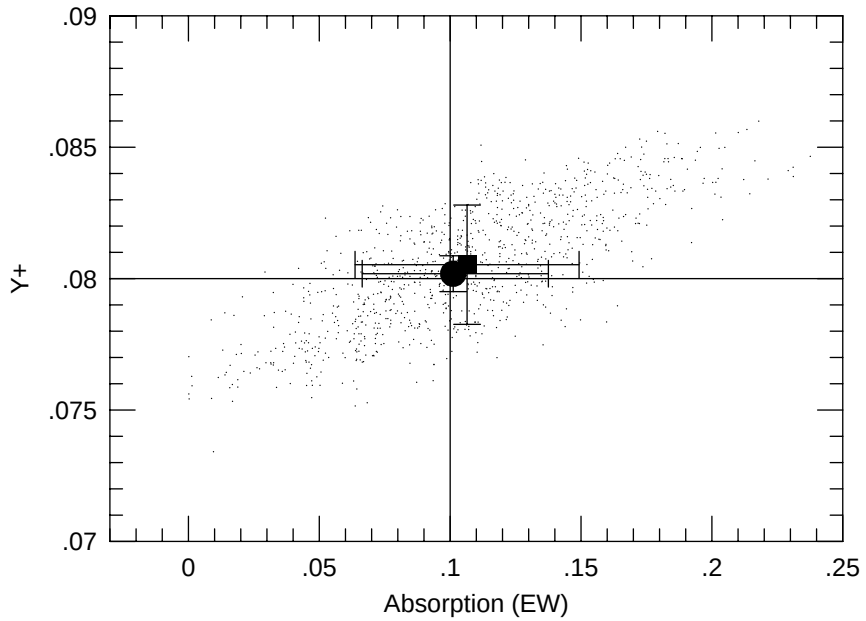


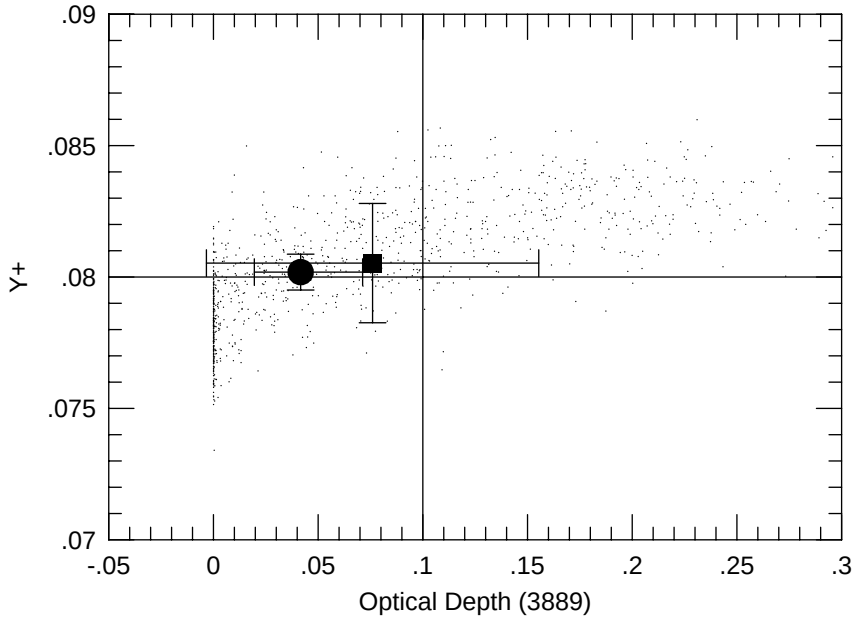


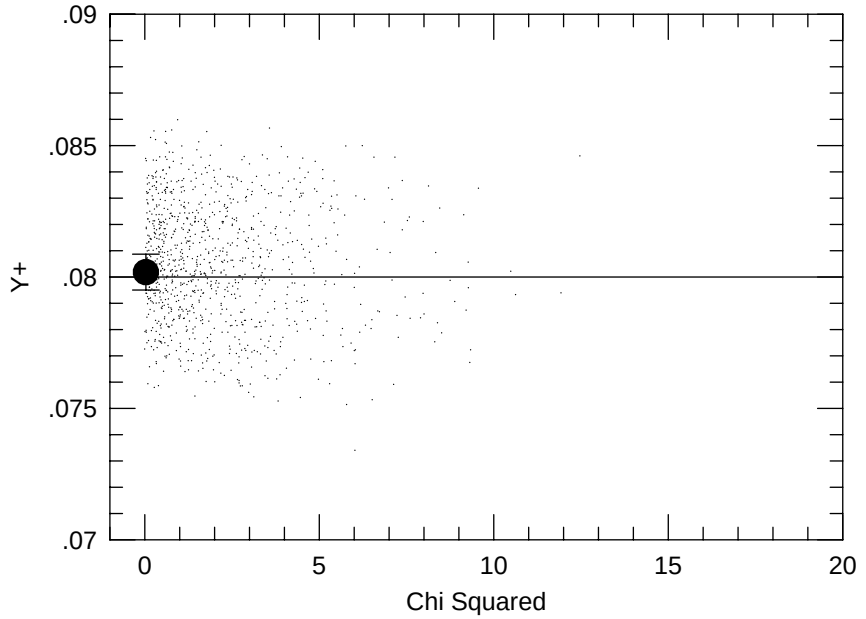

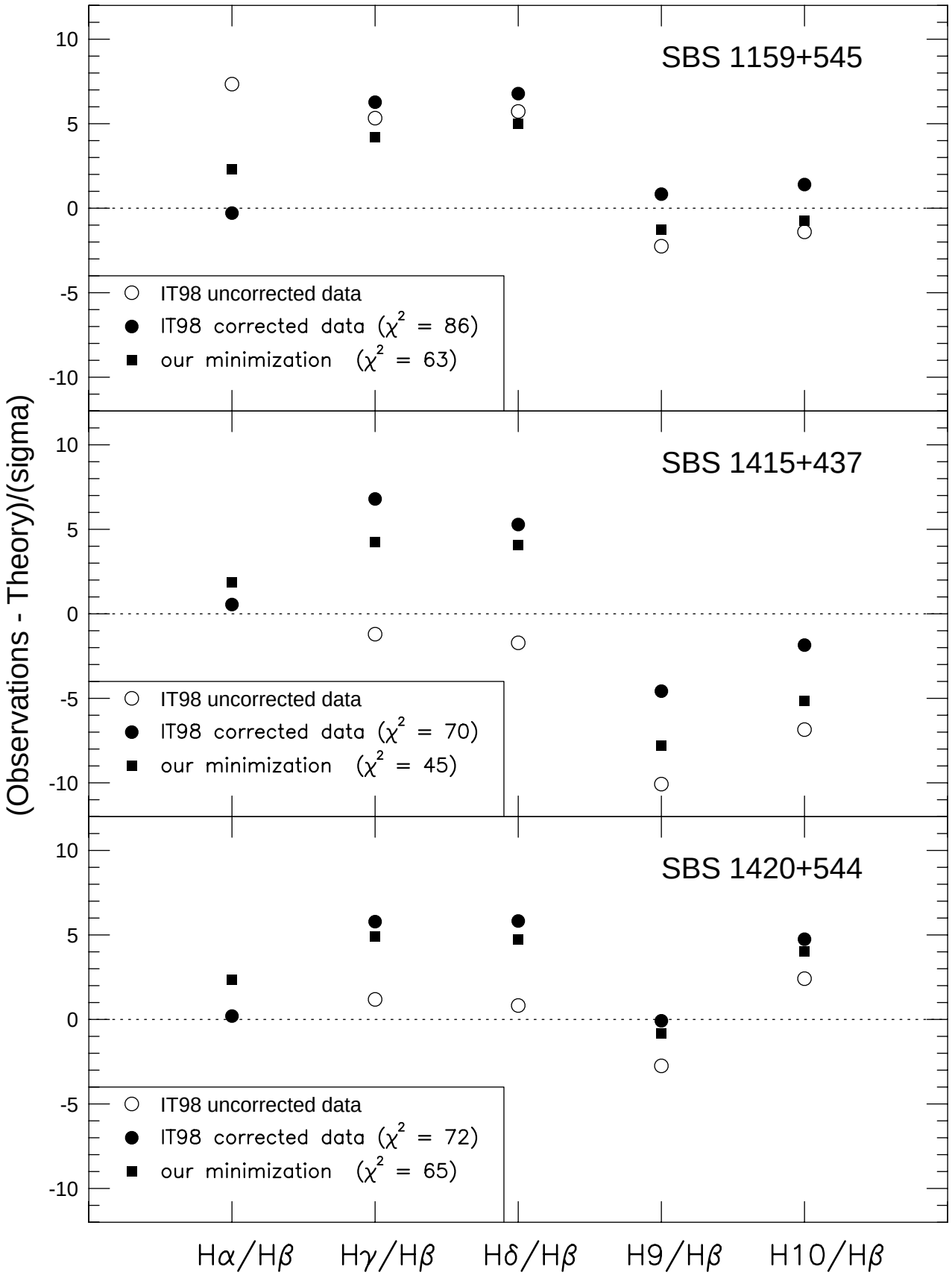
SBS 1159+545
SBS 1415+437
SBS 1420+544
IT98 uncorrected data
IT98 corrected data ($\chi^2$ = 86)
our minimization ($\chi^2$ = 63)
IT98 uncorrected data
IT98 corrected data ($\chi^2$ = 70)
our minimization ($\chi^2$ = 45)
IT98 uncorrected data
IT98 corrected data ($\chi^2$ = 72)
our minimization ($\chi^2$ = 65)
(Observations - Theory)/(sigma)
10
5
0
-5
-10
Hα/Hβ
Hγ/Hβ
Hδ/Hβ
H9/Hβ
H10/Hβ

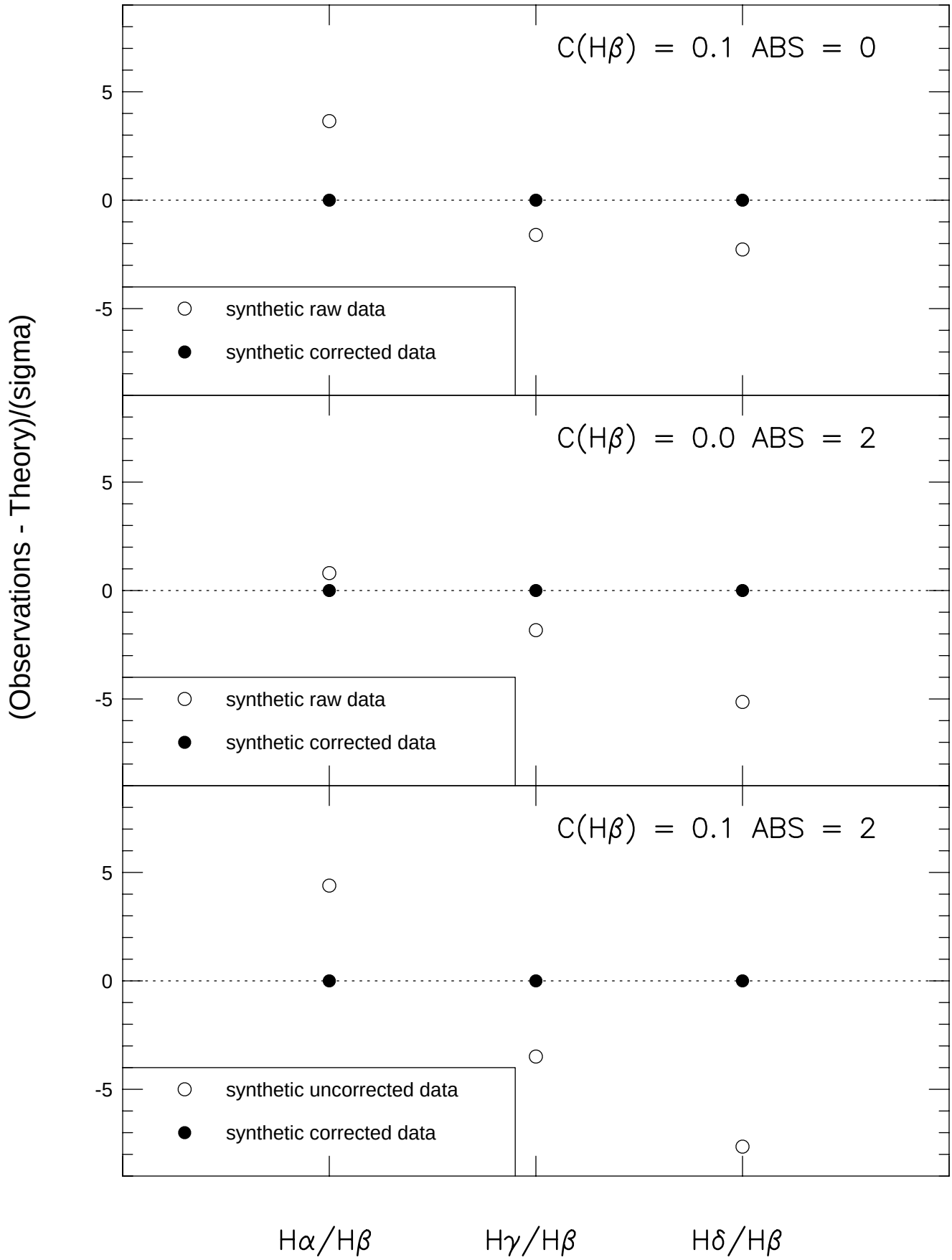
C(Hβ) = 0.1 ABS = 0
C(Hβ) = 0.0 ABS = 2
C(Hβ) = 0.1 ABS = 2
synthetic raw data
synthetic corrected data
synthetic uncorrected data
synthetic corrected data
5
0
-5
(Observations - Theory)/(sigma)
Hα/Hβ
Hγ/Hβ
Hδ/Hβ

# Synthetic Data (T = 1.8, EW(HB) = 100)

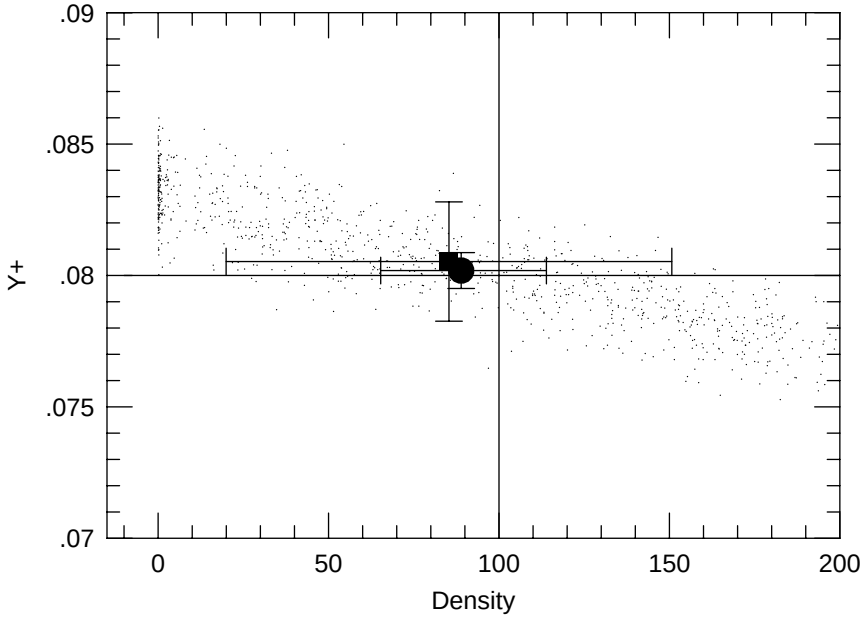


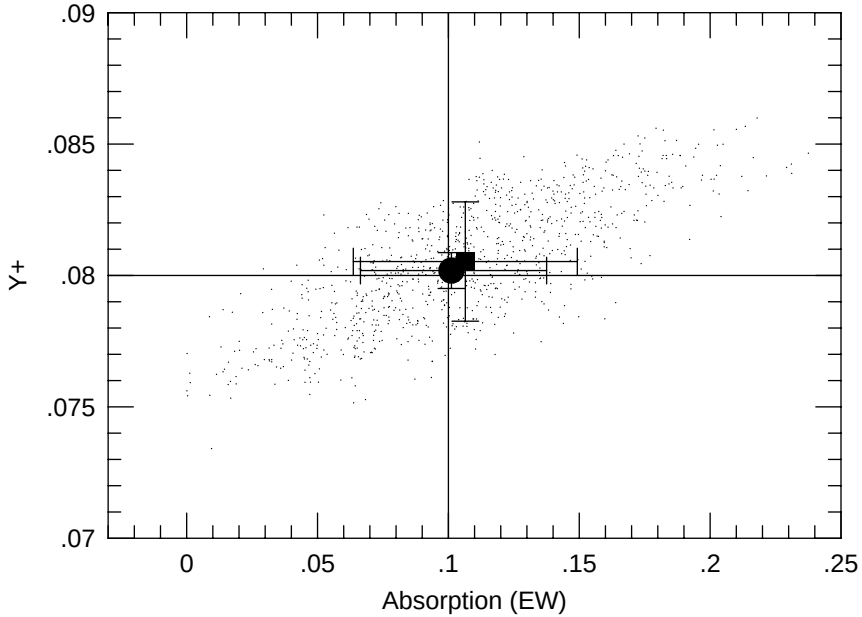


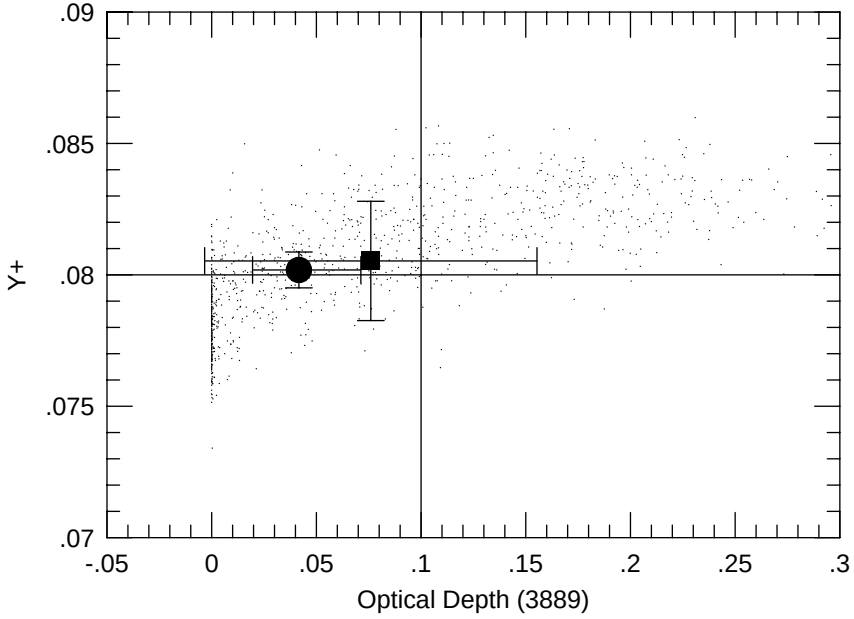


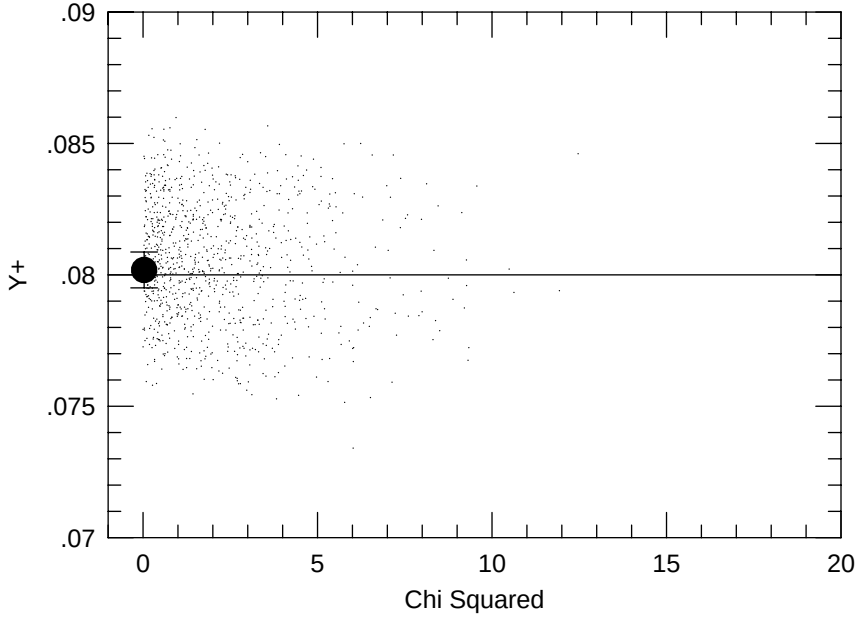

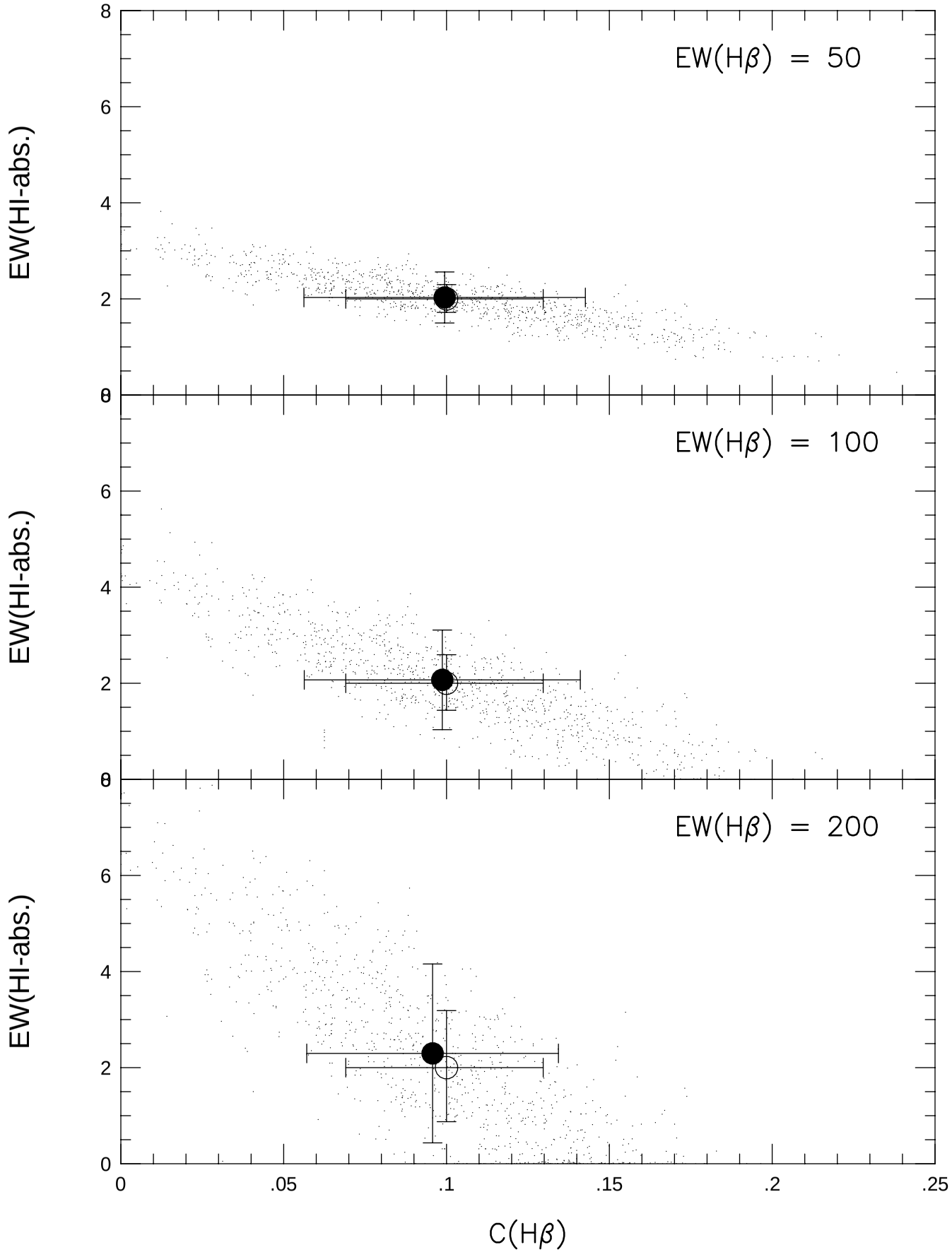
EW(Hβ) = 50
EW(Hβ) = 100
EW(Hβ) = 200
EW(HI-abs.)
EW(HI-abs.)
EW(HI-abs.)
C(Hβ)
0
2
4
6
8
0
.05
.1
.15
.2
.25

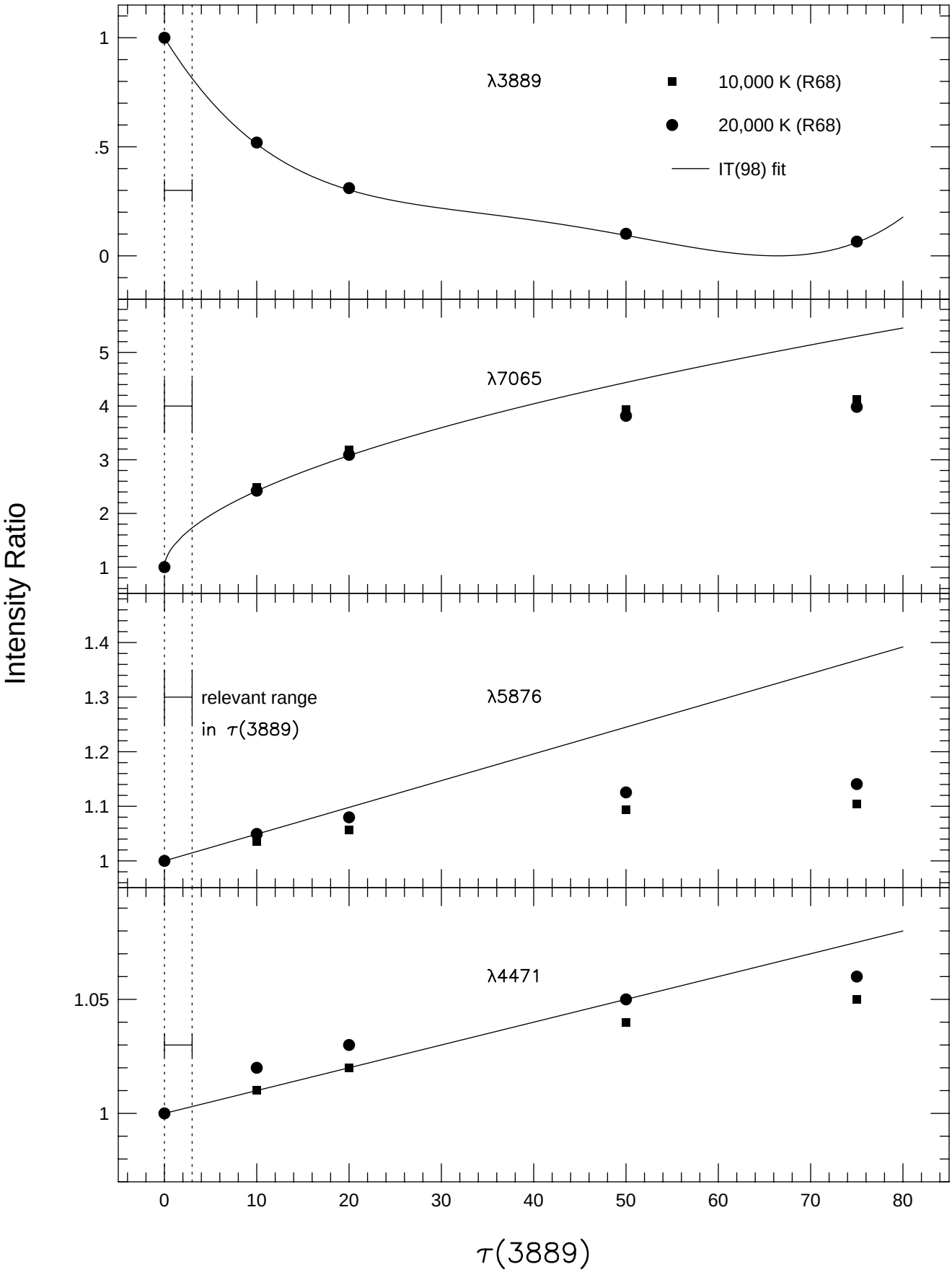
λ3889
10,000 K (R68)
20,000 K (R68)
IT(98) fit
λ7065
relevant range
in τ(3889)
λ5876
λ4471
Intensity Ratio
τ(3889)

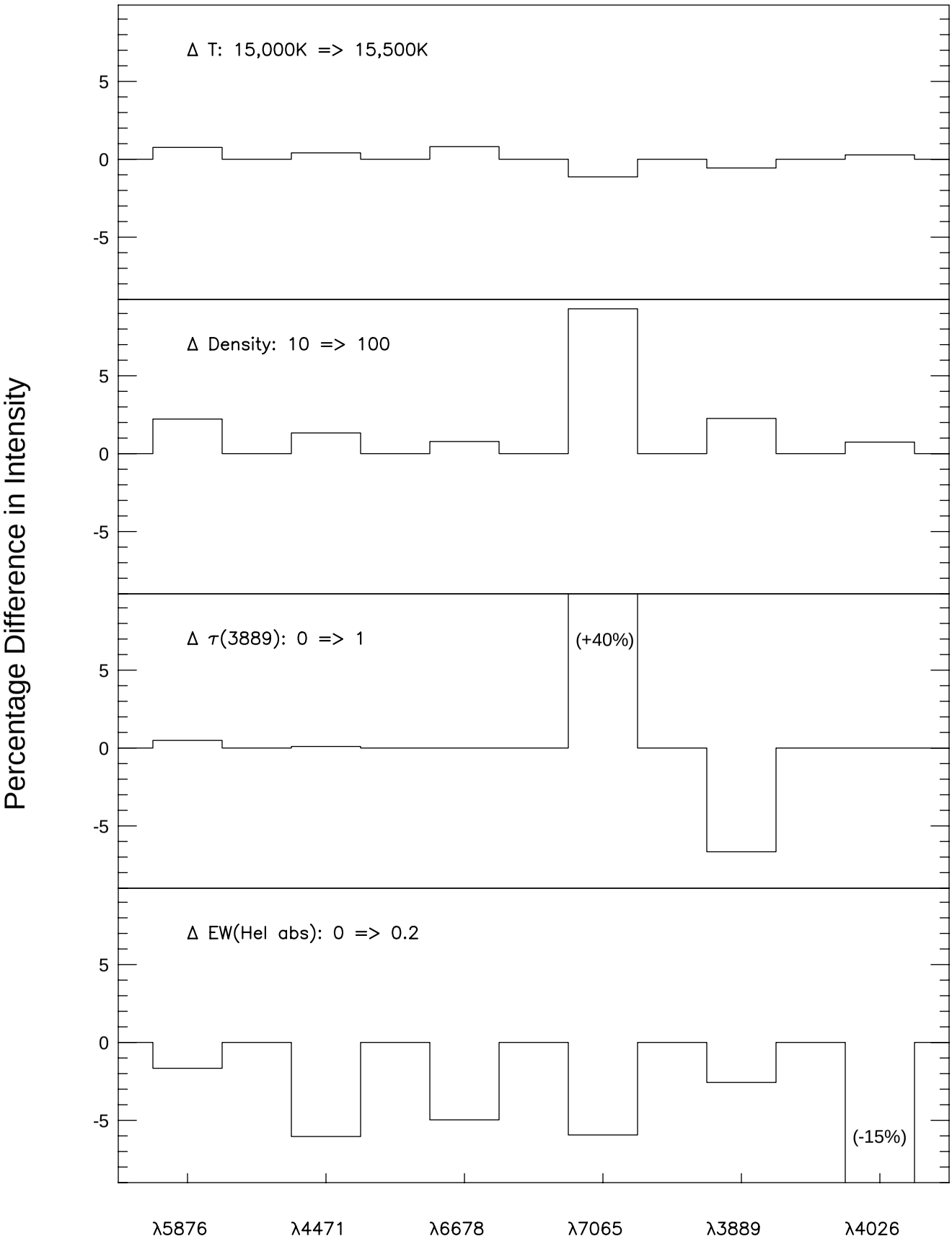
Δ T: 15,000K => 15,500K
Δ Density: 10 => 100
Δ τ(3889): 0 => 1
(+40%)
Δ EW(HeI abs): 0 => 0.2
(-15%)
5
0
-5
Percentage Difference in Intensity
λ5876
λ4471
λ6678
λ7065
λ3889
λ4026

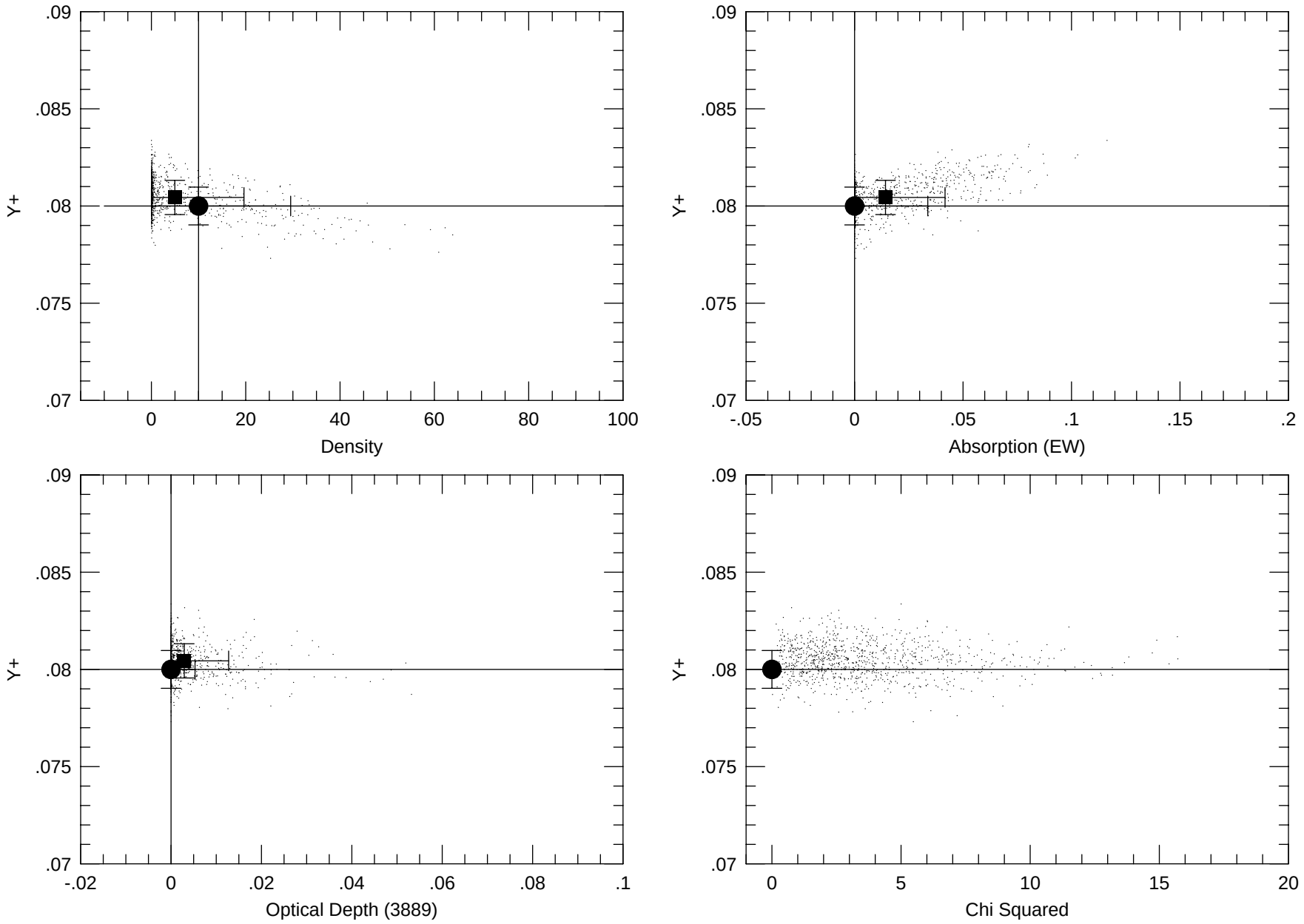
Synthetic Data (T = 1.8, EW(HB) = 100)
Y+
.09
.085
.08
.075
.07
0
20
40
60
80
100
Density
-.05
0
.05
.1
.15
.2
Absorption (EW)
-.02
0
.02
.04
.06
.08
.1
Optical Depth (3889)
0
5
10
15
20
Chi Squared

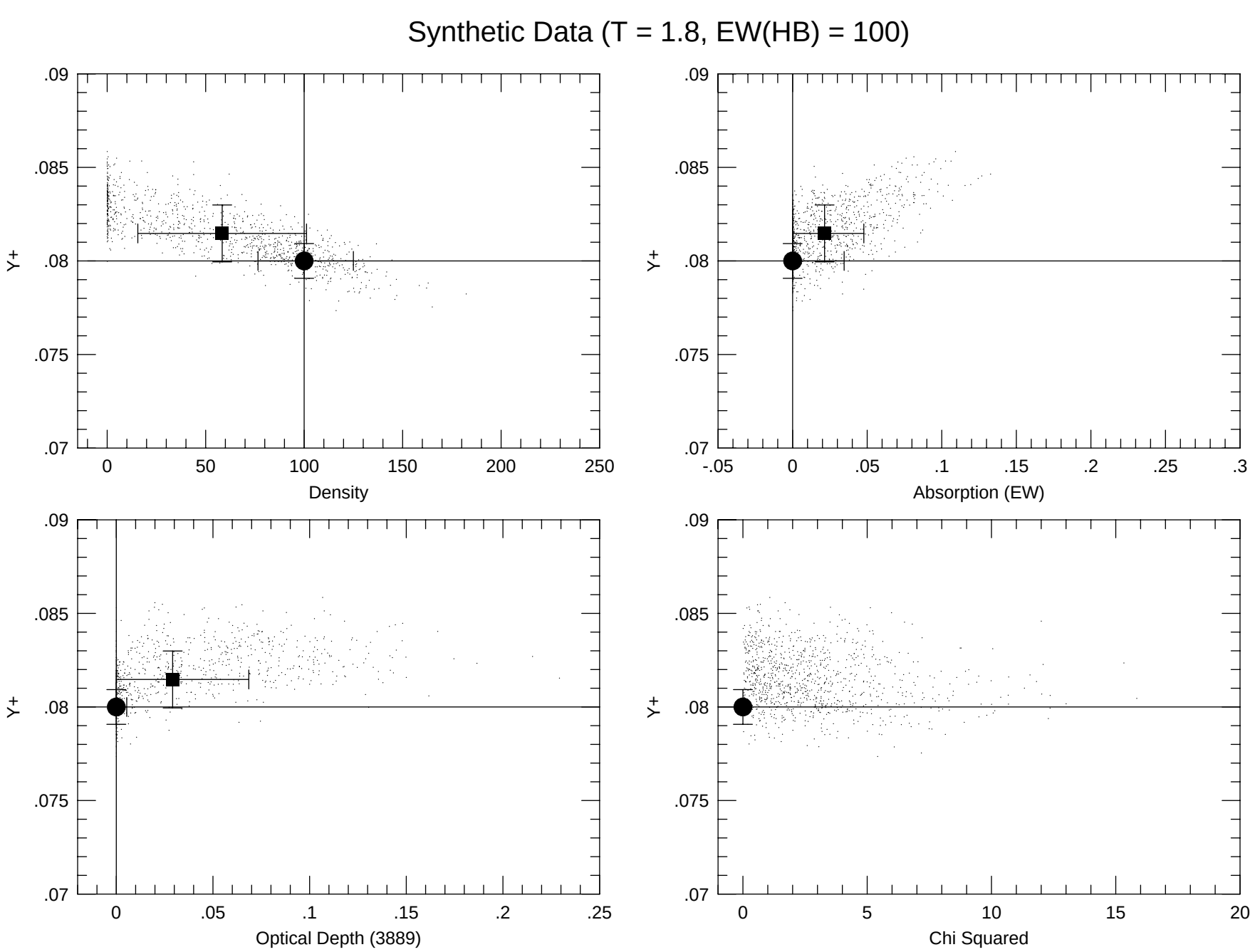
Synthetic Data (T = 1.8, EW(HB) = 100)
Y+
.09
.085
.08
.075
.07
0
50
100
150
200
250
Density
-.05
.05
.1
.15
.2
.25
.3
Absorption (EW)
.25
Optical Depth (3889)
5
10
15
20
Chi Squared

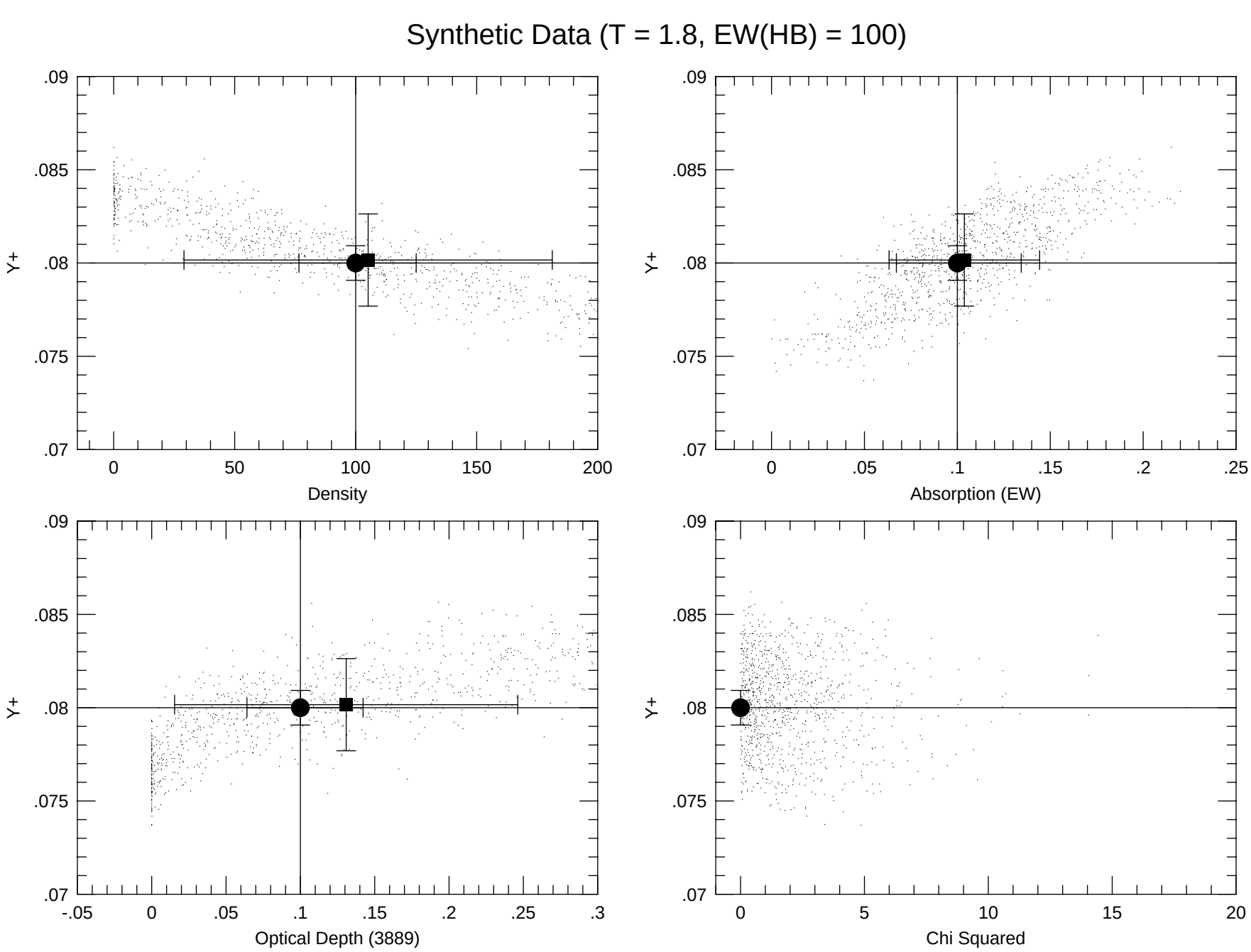
Synthetic Data (T = 1.8, EW(HB) = 100)
Y+
.09
.085
.08
.075
.07
0
50
100
150
200
Density
Absorption (EW)
.05
.1
.15
.2
.25
Optical Depth (3889)
-.05
.3
Chi Squared
5
10
15
20

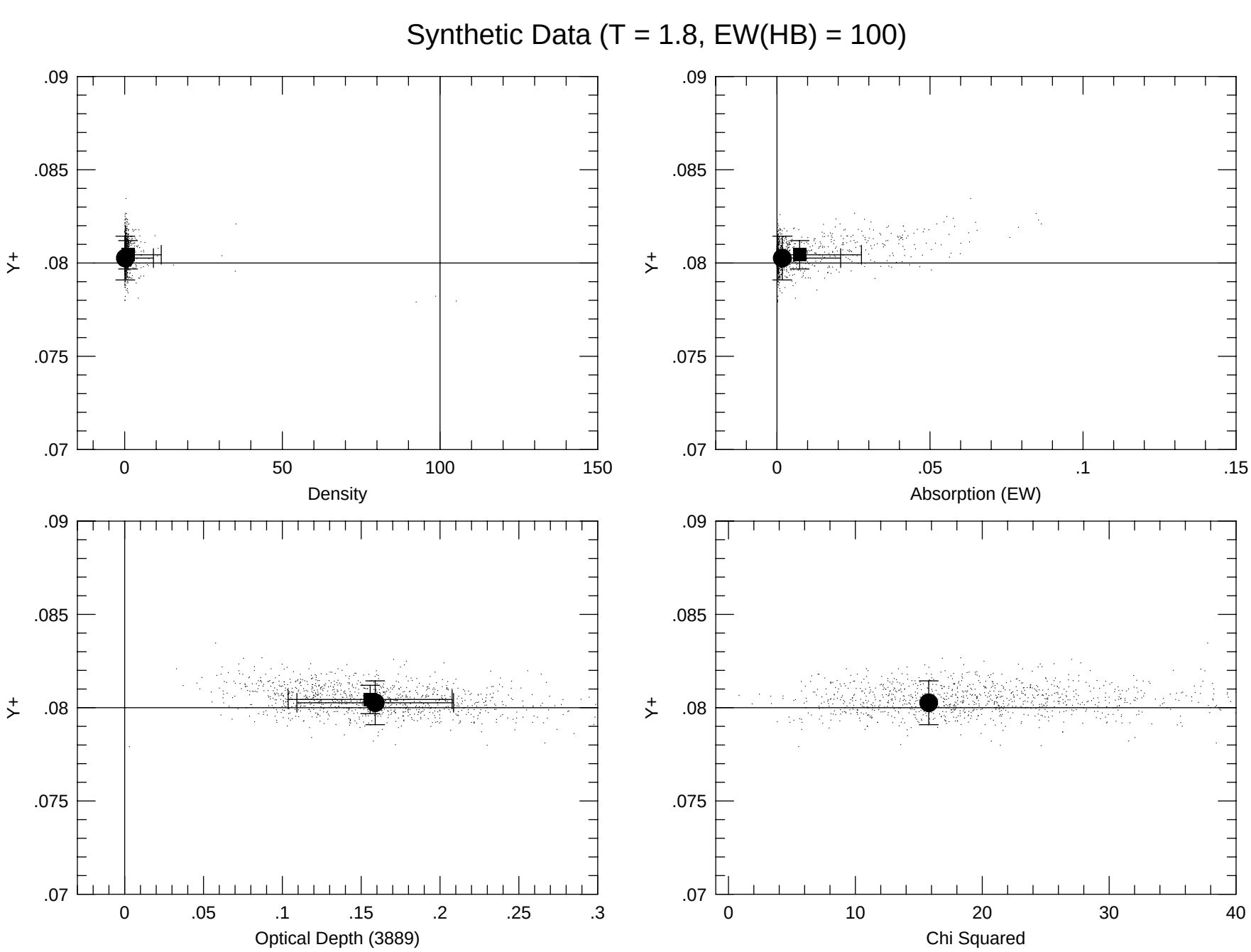
Synthetic Data (T = 1.8, EW(HB) = 100)
.09
.085
.08
.075
.07
Y+
0
50
100
150
Density
0
.05
.1
.15
Absorption (EW)
0
.05
.1
.15
.2
.25
.3
Optical Depth (3889)
0
10
20
30
40
Chi Squared

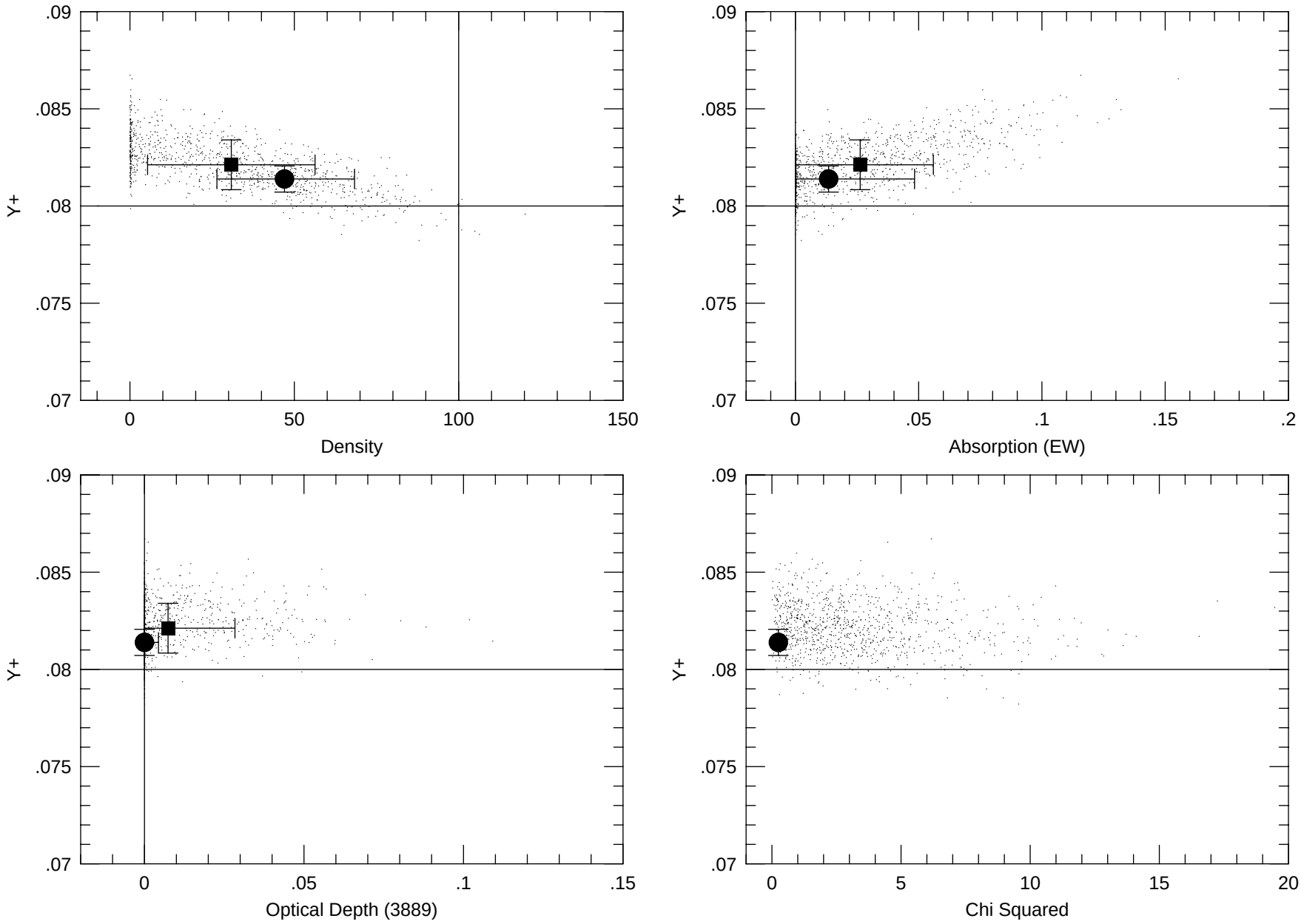
Synthetic Data (T = 1.8, EW(HB) = 100)
.09
.085
.08
.075
.07
Y+
0
50
100
150
Density
0
.05
.1
.15
.2
Absorption (EW)
0
.05
.1
.15
Optical Depth (3889)
0
5
10
15
20
Chi Squared

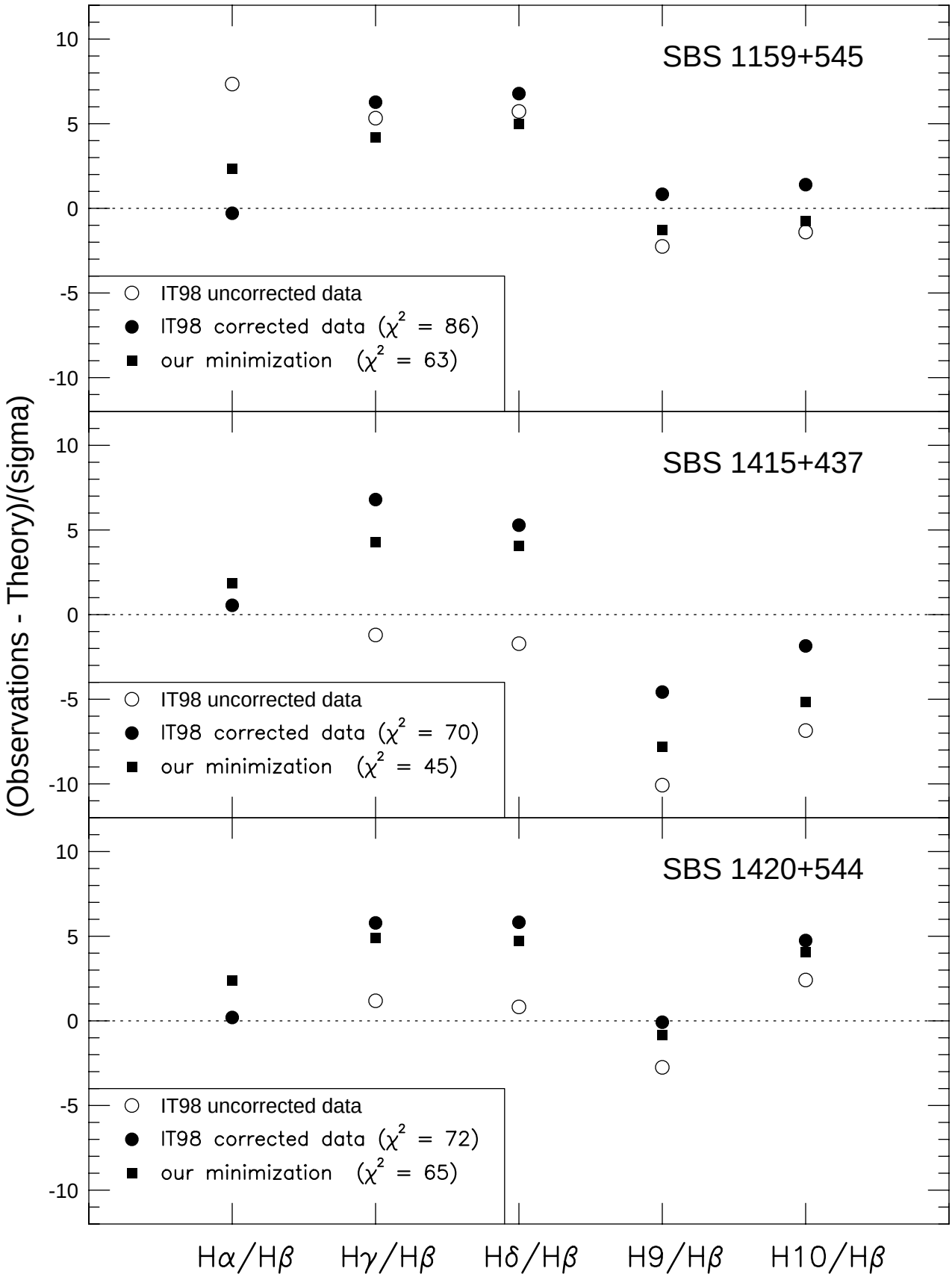
SBS 1159+545
SBS 1415+437
SBS 1420+544
IT98 uncorrected data
IT98 corrected data ($\chi^2$ = 86)
our minimization ($\chi^2$ = 63)
IT98 uncorrected data
IT98 corrected data ($\chi^2$ = 70)
our minimization ($\chi^2$ = 45)
IT98 uncorrected data
IT98 corrected data ($\chi^2$ = 72)
our minimization ($\chi^2$ = 65)
(Observations - Theory)/(sigma)
10
5
0
-5
-10
Hα/Hβ
Hγ/Hβ
Hδ/Hβ
H9/Hβ
H10/Hβ